Politecnico di Torino

Corso di Laura Magistrale in
Ingegneria Energetica e Nucleare

Sustainable Nuclear Energy

Academic Year 2022/2023

Implementation of a reference neutronics calculation scheme with depletion for PWR cores using APOLLO3® code

Academic Tutor:
Prof. Sandra Dulla

Company Tutor:
Nicolas Gerard Castaing

Candidate:
Gianluca Cirillo
s279758

29 November 2023

Ai miei genitori,
che da sempre credono in me.

A me stesso,
per la mia tenacia e forza di volontà.

"Dopo tanta nebbia, a una a una
si svelano le stelle."

Abstract

The aim of this work is the implementation of a reference neutronic calculation scheme, for a Pressurized Water Reactor (PWR) core in 2-D in depletion, using the lattice part of APOLLO3®. The goal is to build a generic and complete scheme that can be used to validate the standard industrial simplified schemes. The ideal validation of these schemes is with Monte Carlo code but it is constrained by large computational cost and limitation in depletion.
APOLLO3® is the new multi-purpose deterministic code developed by the CEA, in partnership with Framatome and EDF. It enables the computation of nuclear cores undergoing different operational conditions, in order to evaluate the physical quantities of interest for the design and operation of nuclear reactors.
The implemented scheme is based on the Method of Characteristics for 281 energy groups mesh for a small core geometry with heavy reflector whose internal part, including the assemblies, is built in APOLLO3® and the outer part by means of the external tool ALAMOS. The crucial point of the implementation is the evaluation of self-shielding on subdomains testing different methods. The reference case, validated with the results of the previous generation code APOLLO2 and the stochastic code TRIPOLI4®, is the less simplified in which the calculation of self-shielding is performed on the whole geometry.
In this work, before the core, two preliminary cases are presented, the cluster 9x9 and the assembly 17x17, for some important aspects and for a first verification.
The scheme is implemented yielding low reactivity discrepancies for the calculation in steady state and even in depletion. However, the most important characteristic to emphasize is that calculating the self-shielding on subdomains, although there is a greater approximation, the computational time is significantly reduced without having a deterioration in the accuracy of the results.

Acknowledgements

This work is the culmination of an internship carried out at the Laboratoire de Protection, d'Etudes et de Conception (LPEC) within the Service d'Études de Réacteurs et des Mathématiques Appliquées (SERMA), a division of CEA Saclay.

I extend my sincere appreciation to my tutor Nicolas Gérard Castaing, for selecting me as his intern. Throughout the duration of my project, his unwavering guidance, extensive discussions, and inspiring environment proved invaluable. His support played a fundamental role in fostering a conducive environment for learning and growth.

I would also like to express my gratitude to Loïc de Carlan, the Head of SERMA, and Amélie Rouchon, the Head of LPEC, for enabling my enriching experience within CEA.

In the end, I would like to thank all the people I met at SERMA with whom I shared this experience and who have enriched my interest in nuclear engineering and the study of neutronics. In particular, a special thanks to the colleagues of "piece 12", especially to Ruggero, Ruben and Marin with whom I shared problems, calculation errors and much more. Without them my experience would not have been so wonderful.

Acknowledgements

In questo lungo e impegnativo percorso di crescita personale e professionale, vorrei dedicare un sentito ringraziamento a tutte le persone straordinarie che hanno reso questo viaggio così speciale.

Innanzitutto, vorrei ringraziare la professoressa Sandra Dulla, per la professionalità e la disponibilità che mi ha concesso e per la passione che mi ha trasmesso.

Un ringraziamento speciale va alla mia famiglia, ai miei genitori e a mio fratello. I loro sacrifici e il loro sostegno instancabile sono stati fondamentali per arrivare fino a qui. La loro dedizione, che si manifesta attraverso l'appoggio incondizionato ad ogni mia scelta, ha plasmato la persona che sono diventato e continuerà a essere il pilastro fondamentale in ogni fase della mia vita.
La riconoscenza che nutro per voi è profonda e indelebile; la vostra presenza è una fonte inesauribile di forza e ispirazione.

A Sonia, la mia dolce compagna di avventure e mia confidente. Grazie per essermi stata accanto nei giorni più difficili, per essere stata la mia costante anche nei momenti bui, per ogni abbraccio che ha lenito le mie fatiche.
Grazie per essere la mia fonte inesauribile di positività e felicità.

Un ringraziamento va anche ai miei cari amici e colleghi. Grazie per le risate, il sostegno e i mille consigli. Grazie perché con voi non mi sono mai sentito fuoriposto o escluso, mi sono sempre sentito a casa. Siete come una seconda famiglia.
Senza di voi non sarebbe stato lo stesso.

Un pensiero infine va sempre a te nonna, che mi osservi da lontato e mi guidi. Spero che tu sia orgogliosa di me.

Grazie di cuore.
Ad maiora.

Contents

List of Figures

List of Tables

Introduction

Nuclear engineering is a specialized field of engineering that focuses on the study, design, development, and application of nuclear technologies. It encompasses a wide range of areas, including nuclear power generation, nuclear medicine, nuclear research, nuclear waste management, and nuclear propulsion, among others.
One of the key tools in nuclear engineering is the use of computational codes, which play a vital role in simulating and analyzing the behavior of nuclear systems. These codes, often referred to as nuclear codes or neutronic codes, utilize mathematical models and numerical methods to solve complex physical equations governing the behavior of neutrons, radiation, and other nuclear processes.
The application of codes in nuclear engineering is multifaceted. In the context of nuclear power generation, neutronic codes are used to design and analyze nuclear reactors, optimizing their performance, safety, and efficiency. These codes help predict reactor behavior, neutron flux distribution, fuel burn-up, and reactor power output, enabling engineers to optimize reactor core configurations and ensure safe and stable operation.
The use of computational codes in nuclear engineering offers several advantages. Firstly, they provide a cost-effective and safe means of conducting virtual experiments and simulations that would be otherwise impractical or hazardous to perform in real-world settings. Secondly, they enable engineers and scientists to optimize designs and explore a wide range of scenarios to identify potential issues and develop suitable solutions.
The Commissariat à l'énergie atomique et aux énergies alternatives (CEA) is actively engaged in developing calculation programs to support the design and operation processes [1]. As part of this effort, the Service d'Etude des Réacteurs et de Mathématiques Appliquées (SERMA) has been working on the creation of a new deterministic neutronics code called APOLLO3® [2]. To ensure the accuracy and reliability of schemes based on this new code, it is essential to perform reference calculations for validation of the standard simplified industrial scheme with depletion, such as diffusion core calculations. One valuable approach to verify the performance of the APOLLO3® code is through the study of a bench-marking case, involving a two-dimensional geometry of a small Pressurized Water Reactor (PWR) core with a heavy reflector for which results from the former generation code APOLLO2 and stochastic code TRIPOLI4® are available.
The main objectives of this internship regards developing a calculation scheme utilizing the lattice part of APOLLO3®, testing different method to evaluate the self-shielding on subdomains. In the implemented calculation scheme, the neutron flux

is solved using the Method of Characteristics, with 281 energy groups.
In this thesis the results of the scheme for some preliminary cases and for the main one of the core are presented and verified, with an introduction reminding the neutronic back-ground and in particular the neutron transport and depletion theory. First, the case under examination, the numerical techniques, the codes and tools used in the study are presented. Then, it is explained step by step the implementation of the calculation scheme and the various methods used in particular for the calculation of self-shielding. After this, the next part focuses on the treatment of the preliminary geometry studied and the final geometry of the core, showing the results used and comparing them with those of APOLLO2 and Tripoli4® for verification and validation.

Chapter 1

Neutron-matter interactions

In this initial chapter some basic elements for the description of nuclear reactor physics will be presented. In order to understand and mathematically define the various aspects, such as power generation and distribution, the study of the properties of materials under neutron irradiation and so on, a model describing neutron behaviour is required. Before defining this mathematical model, it is necessary to recall the basic physical quantities that characterize the study.

1.1 Basic nuclear definitions

In the following section the reader will find basics concepts and definitions. The first quantities to be presented are those that define the physical space that contextualizes the study under examination: it will be indicated with t the time, $\mathbf{r} = (x, y, z)$ the position vector, E the energy, $\mathbf{v}$ the velocity vector and $\mathbf{\Omega} = \frac{\mathbf{v}}{|\mathbf{v}|}$ the vector that describes the direction.

$$\begin{cases} \mathbf{\Omega} = \Omega_x \mathbf{e}_x + \Omega_y \mathbf{e}_y + \Omega_z \mathbf{e}_z \\ \Omega_x^2 + \Omega_y^2 + \Omega_z^2 = 1 \end{cases} \tag{1.1}$$

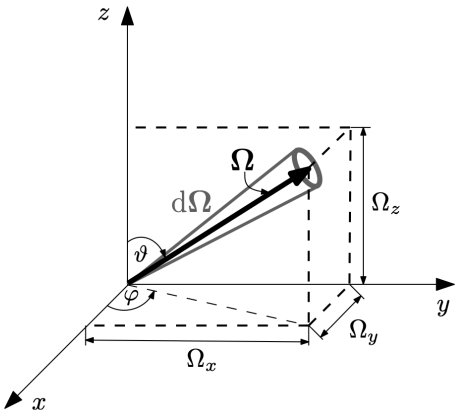

Figure 1.1: Cartesian coordinate reference system [3].

From this last definition, the velocity can be written as $\mathbf{v} = |\mathbf{v}|\mathbf{\Omega}$ ($v = |\mathbf{v}|$).
Now it is possible to define the neutron density function that is a probability density function defined as follows:

$$n(\mathbf{r}, E, \mathbf{\Omega}, t) \tag{1.2}$$

Where the $(\mathbf{r}, E, \mathbf{\Omega})$ is called phase space (Figure 1.2). In order to evaluate the number of neutrons in the small volume $\mathrm{d}\mathbf{r}$, with energy in the range $(E, E + \mathrm{d}E)$, direction $\mathbf{\Omega}$ and at the time t, this function is multiplied by the volume of interest:

$$n(\mathbf{r}, E, \mathbf{\Omega}, t)\,\mathrm{d}\mathbf{r}\,\mathrm{d}E\,\mathrm{d}\mathbf{\Omega} \quad = \quad \text{neutrons within } \mathrm{d}\mathbf{r}\,\mathrm{d}E\,\mathrm{d}\mathbf{\Omega} \tag{1.3}$$

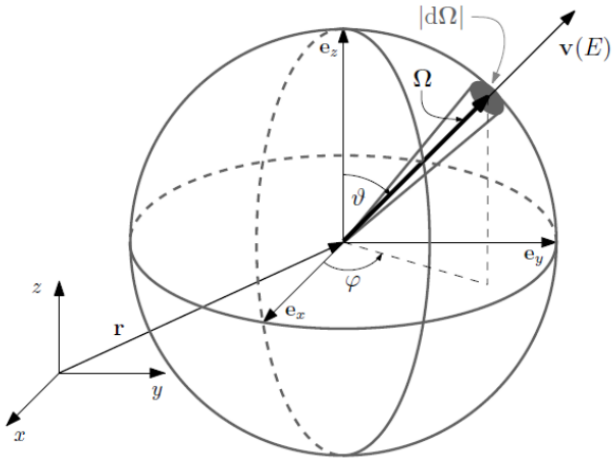

Figure 1.2: Phase space [3].

1.2 Neutron interactions

The main possible different interactions that neutrons can have with the nuclides surrounding them are scattering, capture and fission. Each of these reaction has a possibility to happen; it is possible to indicate with Σ_x the probability per unit path that the event, or collision, "x" occurs and its unit of measurement is cm^{-1}. This quantity is also called macroscopic cross-section. Instead, the microscopic cross section, generally indicated with the symbol σ, is the real area of the target involved in the collision and it is measured in cm^2 or $barn$: if A $[cm^2]$ is the area of a wall, with thickness s $[cm]$, N $[nuclei/cm^3]$ is the particle density and a flux of neutrons passing through it, the probability of collision "x" occurring is assessed as the ratio of the total volume of particles involved and the total volume of the wall.

$$\frac{NAs\sigma_x}{As} = N\sigma_x = \Sigma_x \tag{1.4}$$

The inverse of the macroscopic cross-section $1/\Sigma_x$ is called mean free path.

The number of interactions can be estimated multiplying the total distance travelled by the neutrons and the collision's probability per unit path. The first term is obtained from the multiplication of Equation 1.3 by the neutrons velocity, by dt.

$$n(\mathbf{r}, E, \mathbf{\Omega}, t)\,\mathrm{d}\mathbf{r}\,\mathrm{d}E\,\mathrm{d}\mathbf{\Omega}\,v\,\mathrm{d}t\,\Sigma_x \quad = \quad \text{number of interactions "x"} \tag{1.5}$$

The product of the neutron density function (Equation 1.2) and the speed is defined as angular flux ϕ:

$$\phi(\mathbf{r}, E, \mathbf{\Omega}, t) = n(\mathbf{r}, E, \mathbf{\Omega}, t)v \tag{1.6}$$

Integrating the Equation 1.5 over a defined volume of the phase space, it is possible to evaluate the total number of "x" interactions:

$$\oint \int_E \phi(\mathbf{r}, E, \mathbf{\Omega}, t)\Sigma_x\,\mathrm{d}\mathbf{r}\,\mathrm{d}E\,\mathrm{d}\mathbf{\Omega}\,\mathrm{d}t \quad = \quad \text{total number of interaction "x"} \tag{1.7}$$

As mentioned at the beginning of the section, the main interactions of neutrons are absorption and scattering; the total macroscopic cross-section can be defined as the sum of the cross-section of absorption and scattering.

$$\Sigma_t(\mathbf{r}, E) = \Sigma_a(\mathbf{r}, E) + \Sigma_s(\mathbf{r}, E) \tag{1.8}$$

The cross-sections are not simple constants but they are considered as functions of the position and of the neutron energy colliding on the target. In reality, they depend also on the direction but, in most nuclear engineering cases, the material is considered isotropic so the dependence on $\mathbf{\Omega}$ can be neglected. Concerning the time dependence, furthermore, it is not taken into account because the timescale is relatively much slower than the lifetime of the neutrons and so it is considered only in few relevant cases.
When a neutron is absorbed by a nucleus, a fission or capture event may occur; for absorption it is possible to write:

$$\Sigma_a(\mathbf{r}, E) = \Sigma_c(\mathbf{r}, E) + \Sigma_f(\mathbf{r}, E) \tag{1.9}$$

Concerning the fission, it is defined with $\nu(\mathbf{r}, E)$ the average number of neutrons emitted in $\mathbf{r}$, due to the previous collision on a neutron with energy E', and with $\chi(\mathbf{r}, E)$ the fission spectrum representing the probability density of a produced neutron to be emitted in the energy interval $(E, E + \mathrm{d}E)$. Furthermore, the fission can be considered isotropic and therefore the probability of emitting a neutron in a certain direction is equal to that of all the others $(1/4\pi)$.
If the neutron is not absorbed by a nucleus of the background material, it is simply scattered (deflected) and its direction and energy change; it is possible to write the scattering probability as the sum of the elastic and inelastic scattering probabilities.

$$\Sigma_s(\mathbf{r}, E) = \Sigma_{s,e}(\mathbf{r}, E) + \Sigma_{s,i}(\mathbf{r}, E) \tag{1.10}$$

In addition to knowing the probability that this type of interaction occurs, it is also important to know the probability that a neutron with initial energy E', and with

direction $\mathbf{\Omega}'$, is re-emitted after a scattering event, in a certain cone (solid angle) $\mathrm{d}\mathbf{\Omega}$ with energy in the range $(E, E + \mathrm{d}E)$. For this reason, it can be defined the scattering probability density f_s as probability a density function that depends on the energy before E and after E', and on the direction before $\mathbf{\Omega}'$ and after $\mathbf{\Omega}$ the collision:

$$f_s(\mathbf{r}, E' \to E, \mathbf{\Omega}' \to \mathbf{\Omega}) \tag{1.11}$$

If it is an isotropic medium, the probability density depends not on the two directions, but on the angle formed by these two.

$$f_s(\mathbf{r}, E' \to E, \mathbf{\Omega}' \to \mathbf{\Omega}) = f_s(\mathbf{r}, E' \to E, \mathbf{\Omega}' \cdot \mathbf{\Omega}) \tag{1.12}$$

The scattering probability density may be normalized by the integration over all the directions and over the energy range.

$$\oint \mathrm{d}\mathbf{\Omega} \int_E \mathrm{d}E \, f_s(\mathbf{r}, E' \to E, \mathbf{\Omega}' \to \mathbf{\Omega}) = 1 \tag{1.13}$$

Chapter 2

Neutronics concepts

2.1 The Boltzmann transport equation

The Boltzmann equation, originally formulated by Ludwig Boltzmann, describes the statistical behavior of a gas of particles and the time evolution of their probability distribution function in statistical mechanics [4]. The Neutron Transport equation, also known as the Boltzmann Transport Equation, was later developed in the 20^{th} century to specifically describe the behavior of neutrons in nuclear reactors.
The equation is basically a neutron balance in an infinitesimal volume of phase space ($\mathrm{d}\mathbf{r}\,\mathrm{d}E\,\mathrm{d}\mathbf{\Omega}$); it takes into account neutrons that disappear as a result of interaction with matter (absorption or scattering in another energy group) or losses, and their appearance due, mainly, to fission and scattering.
The variation in time of the neutron angular flux (unknown in the equation) is the sum of all previous contributions.

$$\begin{aligned}\text{neutrons at time } (t+\mathrm{d}t) - \text{neutrons at time } (t) = \\ = (\text{neutrons moving in - neutrons moving out}) + \\ - \text{removal due to collisions} + \\ + \text{neutrons scattered in from outside} + \text{source}\end{aligned}$$

In mathematical form:

$$\begin{aligned}&\frac{1}{v}\frac{\partial}{\partial t}\phi(\mathbf{r},E,\mathbf{\Omega},t) = -\nabla\cdot(\mathbf{\Omega}\phi(\mathbf{r},E,\mathbf{\Omega},t)) - \Sigma_t(\mathbf{r},E)\phi(\mathbf{r},E,\mathbf{\Omega},t) \\ &+ \oint \mathrm{d}\mathbf{\Omega}' \int \mathrm{d}E'\,\Sigma_s(\mathbf{r},E')\phi(\mathbf{r},E',\mathbf{\Omega}',t) f_s(\mathbf{r},E'\to E,\mathbf{\Omega}'\to\mathbf{\Omega}) \\ &+ S(\mathbf{r},E,\mathbf{\Omega},t)\end{aligned} \tag{2.1}$$

This is the integro-differential form of the transport equation. Starting from the left, the first term corresponds to the variation of the neutron population over the time interval $\mathrm{d}t$. The second term represents the net change due to neutrons entering or leaving the volume of the phase space considered and is called streaming term. Then, the third one constitutes the variation due to the absorption and scattering

events, and in particular for the latter, it takes into account those collisions that cause changes in neutron direction and energy (scattering out contribution). The integral term, on the other hand, corresponds to the probability that neutrons with energy E' and direction $\mathbf{\Omega}'$, after a collision, are scattered in the considered volume, assuming energy E and direction $\mathbf{\Omega}$ (scattering in contribution). The last term (S) is the neutron source and it describes the production of neutrons due to an external source or fission phenomena occurring in the reactor, depending if the reactor is in start-up phase or in operation.
Now, if it is considered the most important event of the nuclear engineering, the fission, it is possible to rewrite the equation Equation 2.1 as follows:

$$\begin{aligned}
&\frac{1}{v}\frac{\partial}{\partial t}\phi(\mathbf{r},E,\mathbf{\Omega},t) = -\nabla\cdot(\mathbf{\Omega}\phi(\mathbf{r},E,\mathbf{\Omega},t)) - \Sigma_t(\mathbf{r},E)\phi(\mathbf{r},E,\mathbf{\Omega},t)\\
&+ \oint \mathrm{d}\mathbf{\Omega}' \int \mathrm{d}E'\,\Sigma_s(\mathbf{r},E')\phi(\mathbf{r},E',\mathbf{\Omega}',t) f_s(\mathbf{r},E'\to E,\mathbf{\Omega}'\to\mathbf{\Omega})\\
&+ \oint \mathrm{d}\mathbf{\Omega}' \int \mathrm{d}E'\,\nu(\mathbf{r},E')\Sigma_f(\mathbf{r},E')\phi(\mathbf{r},E',\mathbf{\Omega}',t)\frac{\chi(\mathbf{r},E)}{4\pi} + S(\mathbf{r},E,\mathbf{\Omega},t)
\end{aligned} \tag{2.2}$$

For a steady-state condition, the equation of the particle balance is written removing the time derivative term and removing from each term the dependence on time:

$$\begin{aligned}
&\nabla\cdot(\mathbf{\Omega}\phi(\mathbf{r},E,\mathbf{\Omega})) + \Sigma_t(\mathbf{r},E)\phi(\mathbf{r},E,\mathbf{\Omega}) =\\
&= \oint \mathrm{d}\mathbf{\Omega}' \int \mathrm{d}E'\,\Sigma_s(\mathbf{r},E')\phi(\mathbf{r},E',\mathbf{\Omega}') f_s(\mathbf{r},E'\to E,\mathbf{\Omega}'\to\mathbf{\Omega})\\
&+ \oint \mathrm{d}\mathbf{\Omega}' \int \mathrm{d}E'\,\nu(\mathbf{r},E')\Sigma_f(\mathbf{r},E')\phi(\mathbf{r},E',\mathbf{\Omega}')\frac{\chi(\mathbf{r},E)}{4\pi} + S(\mathbf{r},E,\mathbf{\Omega})
\end{aligned} \tag{2.3}$$

2.1.1 Boundary conditions

Initial and boundary conditions are needed to solve this equation. For what concerns initial conditions, in general it is not restrictive to say that they are known, while boundary conditions require more attention. In particular, the vacuum and symmetry cases are of interest [5]. The first one imposes that if outside the domain there is void (or a rarefied gas), neutrons can leave it but once out they cannot bounce back because they cannot collide anymore, so it is possible to say that the incoming angular flux is equal to zero. The latter, implying a symmetrical geometry, imposes that the incoming angular flux through the border is the same of the angular flux that leaves the border.

$$\begin{cases}
\phi(\mathbf{r},E,\mathbf{\Omega},t=0) = \phi_0(\mathbf{r},E,\mathbf{\Omega}) & \text{(initial condition)}\\
\phi(\mathbf{r},E,\mathbf{\Omega}_{\text{incoming}},t) = 0 & \text{(vacuum BC)}\\
\phi(\mathbf{r},E,\mathbf{\Omega}_{\text{incoming}},t) = \phi(\mathbf{r},E,\mathbf{\Omega}_{\text{outgoing}},t) & \text{(reflective BC)}
\end{cases}$$

2.1.2 The criticality problem: multiplication factor

The criticality problem in nuclear reactor theory is a crucial issue that refers to the situation where, in a system, the neutron disappearance and production rates are balanced, without a substantial increase or decrease in the neutron population. This results in a self-sustaining of the reactor chain and the amount of neutrons remains constant over time. To ensure stationary and continuous energy production through fission reactions, it is necessary to achieve this balance between production and absorption (and leakage). In case this equilibrium occurs, the reactor does not need an external source of neutrons but the only source will be the fission phenomenon. The Equation 2.3 can be written as:

$$\begin{aligned} &\nabla \cdot (\mathbf{\Omega}\phi(\mathbf{r}, E, \mathbf{\Omega})) + \Sigma_t(\mathbf{r}, E)\phi(\mathbf{r}, E, \mathbf{\Omega}) = \\ &= \oint \mathrm{d}\mathbf{\Omega}' \int \mathrm{d}E'\, \Sigma_s(\mathbf{r}, E')\phi(\mathbf{r}, E', \mathbf{\Omega}')f_s(\mathbf{r}, E' \to E, \mathbf{\Omega}' \to \mathbf{\Omega}) \\ &+ \oint \mathrm{d}\mathbf{\Omega}' \int \mathrm{d}E'\, \nu(\mathbf{r}, E')\Sigma_f(\mathbf{r}, E')\phi(\mathbf{r}, E', \mathbf{\Omega}')\frac{\chi(\mathbf{r}, E)}{4\pi} \end{aligned} \tag{2.4}$$

A reactor in this configuration is called critical reactor. If, instead, the number of neutrons produced by fission is lower than those escaped or absorbed, the reactor is in a sub-critical configuration. On the other hand, the number of neutrons produced may exceed those lost and in this case the configuration of the reactor would be super-critical. The criticality problem is approached, from a mathematical point of view, introducing the eigenvalue problem. In fact, it is possible to notice that the time-independent transport equation (Equation 2.4) is of homogeneous type; to evaluate a non-zero solution and to be able to use this equation also for non-critical reactors, which would require a time-dependent equation, the transport equation is transformed into an eigenvalue problem by inserting a constant. The latter is indicated by the letter k and is called multiplication factor.

$$\begin{aligned} &\nabla \cdot (\mathbf{\Omega}\phi(\mathbf{r}, E, \mathbf{\Omega})) + \Sigma_t(\mathbf{r}, E)\phi(\mathbf{r}, E, \mathbf{\Omega}) = \\ &= \oint \mathrm{d}\mathbf{\Omega}' \int \mathrm{d}E'\, \Sigma_s(\mathbf{r}, E')\phi(\mathbf{r}, E', \mathbf{\Omega}')f_s(\mathbf{r}, E' \to E, \mathbf{\Omega}' \to \mathbf{\Omega}) \\ &+ \frac{1}{k}\frac{\chi(\mathbf{r}, E)}{4\pi} \oint \mathrm{d}\mathbf{\Omega}' \int \mathrm{d}E'\, \nu(\mathbf{r}, E')\Sigma_f(\mathbf{r}, E')\phi(\mathbf{r}, E', \mathbf{\Omega}') \end{aligned} \tag{2.5}$$

It is possible to write this last equation in a more concise way, utilizing the operator notation, useful for the treatment of the eigenvalue problem. The following operators are defined:

$$\hat{T} = \nabla \cdot \mathbf{\Omega} + \Sigma_t(\mathbf{r}, E) \qquad \text{Transport operator}$$

$$\hat{\theta}_s = \oint \mathrm{d}\mathbf{\Omega}' \int \mathrm{d}E'\, \Sigma_s(\mathbf{r}, E')f_s(\mathbf{r}, E' \to E, \mathbf{\Omega}' \to \mathbf{\Omega}) \qquad \text{Scattering operator}$$

$$\hat{F} = \frac{\chi(\mathbf{r}, E)}{4\pi} \oint \mathrm{d}\mathbf{\Omega}' \int \mathrm{d}E'\, \nu(\mathbf{r}, E')\Sigma_f(\mathbf{r}, E') \qquad \text{Fission operator}$$

$$\hat{T}\phi(\mathbf{r}, E, \mathbf{\Omega}) = \hat{\theta}_s\phi(\mathbf{r}, E, \mathbf{\Omega}) + \frac{1}{k}\hat{F}\phi(\mathbf{r}, E, \mathbf{\Omega}) \tag{2.6}$$

The effective multiplication factor k allows to balance the number of neutrons emitted by fission so that the system can be treated as critical; At first, it can be defined as the ratio of the number of neutrons present in two successive fission generations:

$$k = \frac{\text{Number of neutrons of one generation}}{\text{Number of neutrons of the previous generation}}$$

In literature, the effective multiplication factor is indicated as k_{eff}. In addition to the above definition, k can also be defined as the ratio between the fission production and the loss due to absorption or leakage [6]. Taking note of all this, it can be noted that if $k_{\text{eff}} = 1$ then the system can be defined as critical, and the number of neutrons of one generation is equal to that of the previous generation; then the chain of reactions is really independent of time. Whether instead $k_{\text{eff}} < 1$, the configuration is sub-critical meaning that the number of neutrons lost is greater than those produced. On the contrary, whether $k_{\text{eff}} > 1$ the system is super-critical and the neutron population has increased compared to the previous generation [7]. In summary:

$$\begin{cases} k_{\text{eff}} < 1 & \text{Sub-critical system} \\ k_{\text{eff}} = 1 & \text{Critical system} \\ k_{\text{eff}} > 1 & \text{Super-critical system} \end{cases}$$

2.2 Multi-group theory

In this section is presented an introduction to the multi-group theory, aimed at the theoretical explanation of energy discretization and why it is used numerical methods for solving the transport equation [8]. The energy distribution of neutrons is an important aspect: during fission phenomena, high-energy neutrons are produced in the range of MeV and are called fast neutrons. These are slowed down due to interactions and reach much lower energy values comparable to that of the medium. They reach energy levels of the order of eV or even $10^{-2}eV$; for this they are called slow or thermal neutrons and the probability of fission by them increases considerably. Thermal reactors, such as PWRs, use this mechanism and are so called because they rely on neutron slowing down up to thermal energy levels to produce fission. It can be understood from all this that the neutron energy range is large and this makes it impossible, from a computational point of view, to solve the energy-dependent transport equation. The basic idea is to introduce an energy mesh, in which each interval is called energy group (g). The different terms of the neutron transport equation are integrated on the energy group.
The angular flux is defined as:

$$\int_{E_{g-1}}^{E_g} \mathrm{d}E\, \phi(\mathbf{r}, E, \mathbf{\Omega}) = \phi^g(\mathbf{r}, \mathbf{\Omega}) \tag{2.7}$$

The streaming term becomes:

$$\int_{E_{g-1}}^{E_g} \mathrm{d}E\, \nabla \cdot (\mathbf{\Omega}\phi(\mathbf{r}, E, \mathbf{\Omega})) = \nabla \cdot (\mathbf{\Omega}\phi^g(\mathbf{r}, \mathbf{\Omega})) \tag{2.8}$$

The removing term is:

$$\int_{E_{g-1}}^{E_g} \mathrm{d}E\, \Sigma_t(\mathbf{r}, E)\phi(\mathbf{r}, E, \mathbf{\Omega}) = \Sigma_t^g(\mathbf{r}, \mathbf{\Omega})\phi^g(\mathbf{r}, \mathbf{\Omega}) \tag{2.9}$$

The scattering term is:

$$\begin{aligned}
&\int_{E_{g-1}}^{E_g} \mathrm{d}E \sum_{g'=1}^{N_g} \oint \mathrm{d}\mathbf{\Omega}' \int_{E_{g'-1}}^{E_{g'}} \mathrm{d}E'\, \Sigma_s(\mathbf{r}, E')\phi(\mathbf{r}, E', \mathbf{\Omega}')f_s(\mathbf{r}, E' \to E, \mathbf{\Omega}' \to \mathbf{\Omega}) = \\
&= \int_{E_{g-1}}^{E_g} \mathrm{d}E \sum_{g'=1}^{N_g} \oint \mathrm{d}\mathbf{\Omega}' \int_{E_{g'-1}}^{E_{g'}} \mathrm{d}E'\, \Sigma_s(\mathbf{r}, E' \to E, \mathbf{\Omega}' \to \mathbf{\Omega})\phi(\mathbf{r}, E', \mathbf{\Omega}') = \\
&= \sum_{g'=1}^{N_g} \oint \mathrm{d}\mathbf{\Omega}'\, \Sigma_s^{g' \to g}(\mathbf{r}, \mathbf{\Omega}' \to \mathbf{\Omega})\phi^{g'}(\mathbf{r}, \mathbf{\Omega}')
\end{aligned} \tag{2.10}$$

The fission term is:

$$\begin{aligned}
&\frac{1}{k} \int_{E_{g-1}}^{E_g} \mathrm{d}E\, \frac{\chi(\mathbf{r}, E)}{4\pi} \sum_{g'=1}^{N_g} \oint \mathrm{d}\mathbf{\Omega}' \int_{E_{g'-1}}^{E_{g'}} \mathrm{d}E'\, \nu(\mathbf{r}, E')\Sigma_f(\mathbf{r}, E')\phi(\mathbf{r}, E, \mathbf{\Omega}') = \\
&= \frac{1}{k} \frac{\chi^g(\mathbf{r}, E)}{4\pi} \sum_{g'=1}^{N_g} \nu^{g'}(\mathbf{r})\Sigma_f^{g'}(\mathbf{r}, \mathbf{\Omega}) \oint \mathrm{d}\mathbf{\Omega}'\, \phi^{g'}(\mathbf{r}, \mathbf{\Omega}')
\end{aligned} \tag{2.11}$$

where the group-averaged (condensed) cross-section Σ_t^g, $\Sigma_s^{g' \to g}$ and $\Sigma_f^{g'}$ are defined to preserve the reaction rate. Considering only the total cross-section, the condensed definition is:

$$\Sigma_t^g(\mathbf{r}, \mathbf{\Omega}) = \frac{\int_{E_{g-1}}^{E_g} \mathrm{d}E\, \Sigma_t(\mathbf{r}, E)\phi(\mathbf{r}, E, \mathbf{\Omega})}{\int_{E_{g-1}}^{E_g} \mathrm{d}E\, \phi(\mathbf{r}, E, \mathbf{\Omega})} = \frac{\int_{E_{g-1}}^{E_g} \mathrm{d}E\, \Sigma_t(\mathbf{r}, E)\phi(\mathbf{r}, E, \mathbf{\Omega})}{\phi^g(\mathbf{r}, \mathbf{\Omega})} \tag{2.12}$$

Two main problems arise from this definition: the first is that the macroscopic cross-section now depends on the direction; the second is that condensation requires knowledge of the flux, unknown of the equation. The solution to these two troubles will be treated in the next chapter concerning the self-shielding formalism.
The complete multi-group steady-state transport equation is:

$$\begin{aligned}
&\nabla \cdot (\mathbf{\Omega}\phi^g(\mathbf{r}, \mathbf{\Omega})) + \Sigma_t^g(\mathbf{r}, \mathbf{\Omega})\phi^g(\mathbf{r}, \mathbf{\Omega}) = \\
&= \sum_{g'=1}^{N_g} \oint \mathrm{d}\mathbf{\Omega}'\, \Sigma_s^{g' \to g}(\mathbf{r}, \mathbf{\Omega}' \to \mathbf{\Omega})\phi^{g'}(\mathbf{r}, \mathbf{\Omega}') + \\
&+ \frac{1}{k} \frac{\chi^g(\mathbf{r}, E)}{4\pi} \sum_{g'=1}^{N_g} \nu^{g'}(\mathbf{r})\Sigma_f^{g'}(\mathbf{r}, \mathbf{\Omega}) \oint \mathrm{d}\mathbf{\Omega}'\, \phi^{g'}(\mathbf{r}, \mathbf{\Omega}')
\end{aligned} \tag{2.13}$$

2.3 Bateman equations

The temporal evolution of radionuclides concentrations during and after reactor irradiation is governed by the Bateman equations. The changes in the concentration of the different isotopes are due to the fact that, in a nuclear core, during the operation of the reactor, materials subjected to the neutron flux react in different ways; this variation can be described by the Bateman equations, knowing the flux and cross-section of all the isotopes present. They constitute a set of first-order differential equations, in number equal to that of the isotopes contributing in the various decay chains.
The general formula of Bateman equation, for an isotope i, is reported below:

$$\begin{aligned}\frac{\mathrm{d}N_i}{\mathrm{d}t}(\mathbf{r},t) = &-\sum_{j\neq i}\left[\lambda_{ji}^{d} + \int \phi(\mathbf{r},E,t)\sigma_{ji}^{tr}(E)\,\mathrm{d}E\right]N_i(\mathbf{r},t)\\ &+\sum_{j\neq i}\left[\lambda_{ij}^{d} + \int \phi(\mathbf{r},E,t)\sigma_{ij}^{tr}(E)\,\mathrm{d}E\right]N_j(\mathbf{r},t)\end{aligned} \tag{2.14}$$

Where:

- N_i: the concentration of isotope i;
- λ_{ji}^{d}: the decay constant from isotope i to an isotope j;
- σ_{ji}^{tr}: the cross-section of transmutation from isotope i to an isotope j.

The first term in brackets physically represents the disintegration of the i-th nuclide while the second equivalent term represents the unit-time production of the same i-th nuclide, as a result of the disintegration of another j-th nuclide. Each of these two terms is defined as the sum of two different phenomena; the first represents the disintegration of the nuclide by decay and the second is due to the interaction of the nuclide with the particles flux ϕ (in our case neutrons) [9].
The method for solving this set of differential equations of the first order will be presented in the next chapter concerning the type of numerical method used.

2.4 Equations coupling

One of the presumptions that can be used to describe a nuclear core in depletion is that the core is essentially static for the duration of sub-steps in the depletion process. This indicates that the neutronics quantities determined by a transport solver are either constant or exhibit behavior that may be easily interpolated over a time period. The flux solver and the depletion solver can therefore be distinguished from one another. The Bateman equations would be used to compute the depletion and define new isotope concentrations after the Boltzmann equation is applied to describe the reactor's static state and compute the reaction rates and flux.

Chapter 3

Numerical methods

This chapter presents the two macro-families of numerical methods for the study of neutronics. In particular, in the following sections, it will focus on the explanation of the techniques implemented in the code used for the case study of this work.

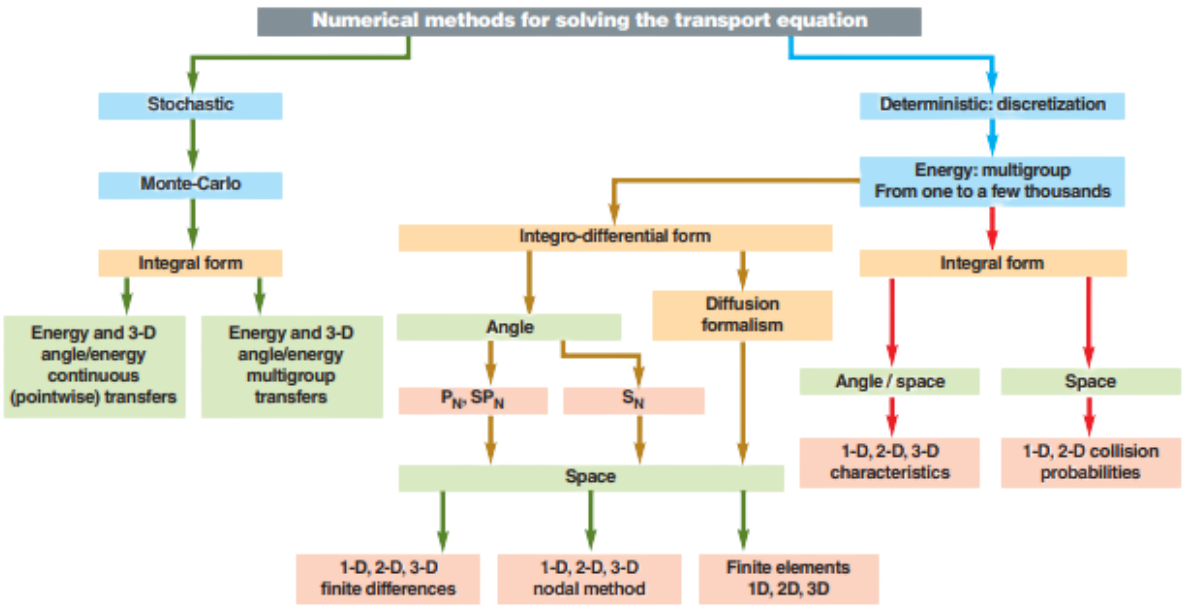

Figure 3.1: Classification of the numerical methods for solving the transport equation [10].

3.1 Deterministic neutronics methods

Deterministic neutronic codes work by solving the neutron transport equation or diffusion equation (simplified form of the previous one), which describes the behavior of neutrons in a nuclear system. A deterministic scheme discretizes all the variables of the equation, which are energy, direction, space and time. By solving these equations, the code can calculate and compute key parameters like neutron

flux distribution, reaction rates, and power distribution using a variety range of numerical techniques. This section will describe only the methods that are available in the deterministic code used and in particular those utilized in the implemented calculation scheme [10].

3.1.1 Flux solver

Method of Characteristics

The Method of Characteristics or MOC is a technique that allows to solve first-order partial differential equation (PDE) by finding curves, called characteristics, along which the PDE behaves like an ordinary differential equation (ODE). The search for characteristic curves then results in the use of a new coordinate system. Once the ODE is found, it is resolved along the characteristics and transformed into a solution for the PDE. This method is one of the most effective computational techniques for solving transport-type differential equations, due to its discretization. It is widely utilized in industrial calculations due to its ability to strike a balance between accuracy and computational time. Additionally, it offers the advantage of accurately operation on an unstructured 2D mesh and for any arbitrary order of scattering anisotropy.
The MOC is based on a discretization of space, which divides the considered domain into homogeneous regions, and an angle discretization thanks to the method of discrete ordinates.
Below, it is shown the MOC for one of the energy groups (g) in which the energy range is discretized. The subscript is reported only once and then removed to simplify the notation.

$$\boldsymbol{\Omega} \cdot \nabla \phi_g(\mathbf{r}, \boldsymbol{\Omega}) + \Sigma_g(\mathbf{r}) \phi_g(\mathbf{r}, \boldsymbol{\Omega}) = q_g(\mathbf{r}, \boldsymbol{\Omega}) \tag{3.1}$$

Where $q_g(\mathbf{r}, \boldsymbol{\Omega})$ is the source term of the equation.
Space discretization: the considered geometrical domain D is subdivided in a collection I of small homogeneous portions D_i.

$$D = \bigcup_{i=1,I} D_i$$

For each region the source term and the cross sections are considered constant respect to the space:

$$\begin{cases} \Sigma(\mathbf{r}) = \Sigma_i & \forall \mathbf{r} \in D_i, i = 1, I \\ q(\mathbf{r}, \boldsymbol{\Omega}) = q_i(\boldsymbol{\Omega}) \end{cases} \tag{3.2}$$

Angle discretization: the S_N method takes into account a discrete set of directions which approximate the angular domain. Each discrete direction has a weight function:

$$\{\boldsymbol{\Omega}_n, \omega_n\} \quad n = 1, N$$

For the integration on the angular domain is used the so-called quadrature formula that is shown for a generic function:

$$\int_{4\pi} f(\mathbf{\Omega})\,\mathrm{d}\mathbf{\Omega} = \sum_{n=1}^{N} \omega_n f(\mathbf{\Omega}_n) \tag{3.3}$$

The direction of the straight line k is $\mathbf{\Omega}$ while $\mathbf{\Omega}_\perp$ is its perpendicular direction; it is possible to write all the points of the characteristic line k as:

$$\mathbf{r} = s_{\perp k}\mathbf{\Omega}_\perp + s\mathbf{\Omega}$$
$$\mathbf{r}_{0k} = s_{\perp k}\mathbf{\Omega}_\perp$$

Where $s_{\perp k}$ characterizes the track k and where s is the curvilinear axis of the characteristic curve. Now, the unknown of the problem are the values on the angular flux in these directions considered.

$$\frac{\mathrm{d}\phi(\mathbf{r}_{0k} + s\mathbf{\Omega}, \mathbf{\Omega})}{\mathrm{d}s} + \Sigma(\mathbf{r}_{0k} + s\mathbf{\Omega})\phi(\mathbf{r}_{0k} + s\mathbf{\Omega}, \mathbf{\Omega}) = q(\mathbf{r}_{0k} + s\mathbf{\Omega}, \mathbf{\Omega}) \tag{3.4}$$

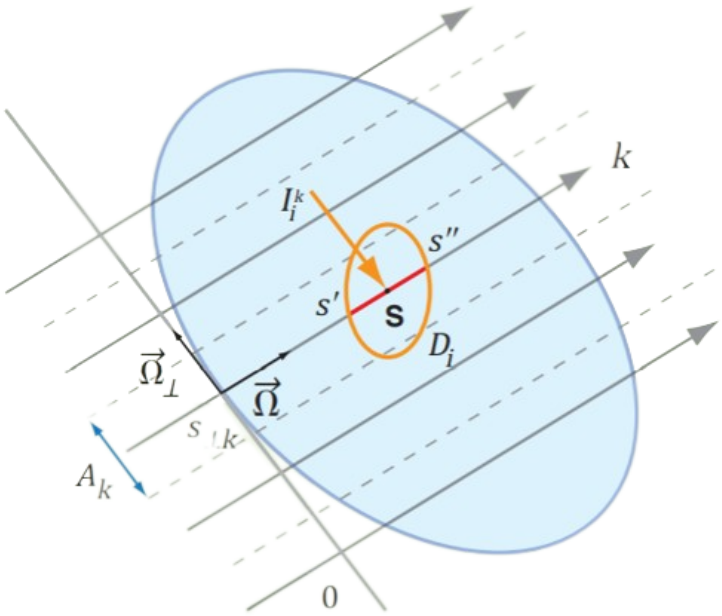

Figure 3.2: MOC: Space and angle discretization [10].

The analytical solution of the characteristic equation Equation 3.4 along the straight lines k for each point $\mathbf{r}_{0k} + s\mathbf{\Omega}$ is obtained by integrating on the computational domain D_i and is expressed as a function of the analytical solution at the entry point $\mathbf{r}_{0k} + s'\mathbf{\Omega}$:

$$\phi(\mathbf{r}_{0k} + s\mathbf{\Omega}, \mathbf{\Omega}) = \phi(\mathbf{r}_{0k} + s'\mathbf{\Omega}, \mathbf{\Omega})e^{-\tau(s)} + \int_{s'}^{s} \mathrm{d}s_1\, q(\mathbf{r}_{0k} + s_1\mathbf{\Omega}, \mathbf{\Omega})e^{-\tau(s_1)} \tag{3.5}$$

τ is the optical path length, representing the probability of a neutron to move from s' to a generic point s without colliding. It is expressed as:

$$\tau(s) = \int_{s'}^{s} \mathrm{d}s_1 \, \Sigma(\mathbf{r}_{0k} + s_1 \mathbf{\Omega}) \tag{3.6}$$

Introducing the hypotheses 3.2, which specify that the cross-section and the source are constant with respect to space in the region considered D_i , the above equation (Equation 3.5) becomes:

$$\phi(\mathbf{r}_{0k} + s\mathbf{\Omega}, \mathbf{\Omega}) = \phi(\mathbf{r}_{0k} + s'\mathbf{\Omega}, \mathbf{\Omega}) e^{-\Sigma_i (s-s')} + \frac{q_i(\mathbf{\Omega})}{\Sigma_i} \Big(1 - e^{-\Sigma_i (s-s')} \Big) \tag{3.7}$$

By choosing an exit point $(\mathbf{r}_{0k} + s''\mathbf{\Omega})$ form the region D_i, it is possible to rewrite the equation as:

$$\phi(\mathbf{r}_{0k} + s''\mathbf{\Omega}, \mathbf{\Omega}) = \phi(\mathbf{r}_{0k} + s'\mathbf{\Omega}, \mathbf{\Omega}) e^{-\Sigma_i I_i^k} + \frac{\Big(1 - e^{-\Sigma_i I_i^k} \Big)}{\Sigma_i} q_i(\mathbf{\Omega}) \tag{3.8}$$

Where $I_i^k = s'' - s'$ and the Equation 3.8 is called "transmission equation". In order to obtain an average information on the whole characteristic line, it is possible to mediate the previous equation on the optical path:

$$\bar{\phi}_i^k = \frac{\phi(\mathbf{r}_{0k} + s'\mathbf{\Omega}, \mathbf{\Omega}) - \phi(\mathbf{r}_{0k} + s''\mathbf{\Omega}, \mathbf{\Omega})}{\Sigma_i I_i^k} + \frac{q_i(\mathbf{\Omega})}{\Sigma_i} \tag{3.9}$$

This equation is called "balance equation" and thanks to it an average value of the flux along the path can be obtained, while ensuring that the right number of neutrons is considered.
The Equation 3.8 and Equation 3.9 give an information about the angular flux on the characteristic line with $\mathbf{\Omega}$ direction. Transverse integration must be considered to obtain an average value of the flux over the entire geometry.
The average angular flux, on the discretized domain D_i with volume V_i, is expressed:

$$\begin{aligned} \bar{\phi}_i(\mathbf{\Omega}) &= \frac{1}{V_i} \int \mathrm{d}V \, \phi(s_\perp \mathbf{\Omega}_\perp + s\mathbf{\Omega}, \mathbf{\Omega}) = \\ &= \frac{1}{V_i} \int \mathrm{d}s_\perp \int \mathrm{d}s \, \phi(s_\perp \mathbf{\Omega}_\perp + s\mathbf{\Omega}, \mathbf{\Omega}) \end{aligned} \tag{3.10}$$

The quadrature formula is used to perform the approximation of this integral. A set of lines k, defining a tube of transverse section A_k and average flux $\bar{\phi}_i^k$, examines the volume D_i. Therefore, summing the contributions of the character lines k, which are parallel to $\mathbf{\Omega}$ and intercept the region considered, the mean value $\bar{\phi}_i$ can be estimated through the formula:

$$\bar{\phi}_i = \frac{\sum_k A_k I_i^k \bar{\phi}_i^k}{\sum_k A_k I_i^k} \tag{3.11}$$

Collision Probability method

The Collisions Probability method or Pij method is a method that solves the integral transport equation, for each energy group, using the hypothesis of a flat and isotropic source. The result of this technique is a matrix, which binds the neutron flux to this source, and the different elements can be considered as collision probabilities. The evaluation of the matrix , as for the previous method, utilizes parallel characteristics lines for a finite group of angular directions.
For a 3-D geometries and for the same division in subdomains the results of the this method is the same of the MOC. On the contrary, the equivalence between the two methods is not exact in 2-D problems. In this case, the Collision Probability method, to integrate the dependence on the polar angle, uses particular functions, called Bickley-Naylor functions. The same dependence in the MOC is solved by a numerical integration on the angle.
In addition to the hypotheses 3.2, the Collision Probability method considers an isotropic emission and this limits its application to cases with scattering anisotropy order not too high, in particular to cases that can be approximated using zero-order transport correction.
One of the solvers implemented in APOLLO3® using the collission probabily method is the Multicell approximation. Assuming that the intercell interactions can be adequately represented using the spatial uniform and isotropic or linear anisotropic neutronic current approximations, this method offers a highly effective approach for computing matrix coefficients. Under this premise, the matrices are computed individually for each cell with an open boundary condition. However, for identical cells sharing the same spatial mesh and cross sections, the matrix calculation is performed only once. This strategy optimizes computational efficiency while still maintaining a satisfactory level of precision in describing cell interactions.
The concept of cell grouping is introduced by assuming an equivalent flux solution in two or more separate yet optically identical cells. This principle is exemplified by the annular mesh arrangement of fuel pins, where identical region numbering is applied, thereby ensuring the application of the same cell coefficients across all cells within a group.
This approach yields a significant reduction in problem complexity, effectively diminishing the overall computational load. However, it's essential to recognize that cell grouping extends to the grouping of cell surfaces as well. Consequently, a cell belonging to a group may come into contact with more cells than its actual count of neighbors, potentially exerting a notable influence on the transport phenomena within the assembly. Careful consideration is thus warranted to comprehend the implications of cell grouping on transport effects and accuracy [11].

3.1.2 Self-shielding formalism

In general, self-shielding refers to the phenomenon where a material's ability to interact with particles or radiation is affected by its own composition. It occurs when the presence of certain isotopes or elements within a material alters its absorption or scattering characteristics for incoming particles. It is particularly significant in

nuclear reactor analysis and nuclear fuel design. The energy range covered in thermal reactors also includes the resonance zones of different isotopes; resonances are peak in the cross-sections for certain incident particle energy values.

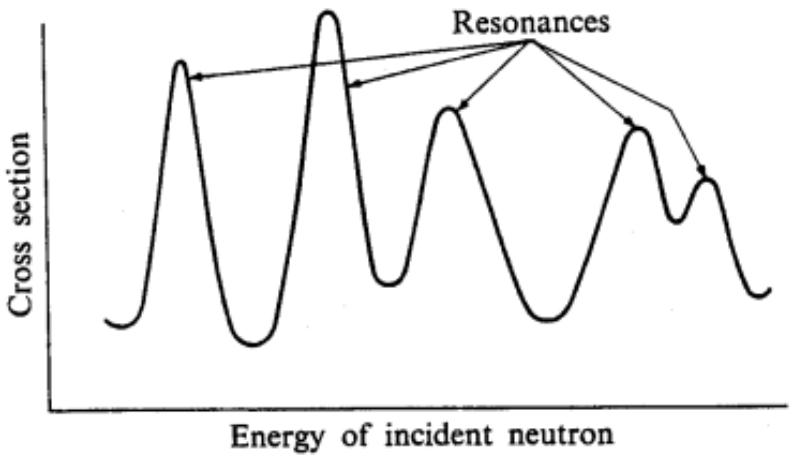

Figure 3.3: Resonances in the cross-section [12].

When a neutron (incident particle in nuclear reactors) has an energy close to that of resonances, the probability of the latter being absorbed increases, thus causing a depression in the neutron flux; this reduction in the energy-dependent flux causes a decrease in actual absorption per nucleus and this effect is the so called energy self-shielding. In nuclear reactors, fuel contains isotopes such as U238 and Pu239 in which the absorption spectrum has resonances at specific energy values. The presence of these resonances, influencing the neutron flux, alters the behavior of neutrons in general and the overall reactivity value.
For this reason, in a neutronics calculation scheme, it is important to take this aspect into account, which cannot be considered negligible especially in deterministic models where a discretization in energy is carried out. To consider the self-shielding phenomenon, an average cross-section on the energy range could be evaluated but weighing it adequately so as not to overestimate the effect of the resonances on the reaction rates; the most appropriate method is to use as a weight function the angular flux for each energy group, as shown by the following equation.

$$\Sigma_g(\mathbf{r}, \mathbf{\Omega}) = \frac{\int_{E_{g-1}}^{E_g} \mathrm{d}E\, \Sigma(\mathbf{r}, E)\phi(\mathbf{r}, E, \mathbf{\Omega})}{\int_{E_{g-1}}^{E_g} \mathrm{d}E\, \phi(\mathbf{r}, E, \mathbf{\Omega})} \tag{3.12}$$

However, the main challenge is that neutron flux is an unknown when calculating self-shielding. For this reason it is possible to replace it with the energy spectrum; a Maxwellian spectrum can be used for the thermal region, a slowing down spectrum for the epithermal range and the fission spectrum for the higher energy ranges.
In order to evaluate the reaction rate, a slowing-down model can be adopted under the hypothesis of elastic and isotropic scattering; the Livolant-Jeanpierre formalism [13] is based on the equivalence between the simplified slowing-down phenomenon

in an infinite homogeneous medium and that in the real heterogeneous geometry. Then, an inverse equivalence is perform to evaluate the cross-section preserving that values of reaction rate.
The set of regions of geometry that share the same resonant mix of isotopes is the so-called self-shielding region on which the calculation is made. Since multi-group reaction rate and flux are space dependent, it is impossible to define once and for all self-shielding cross-sections.

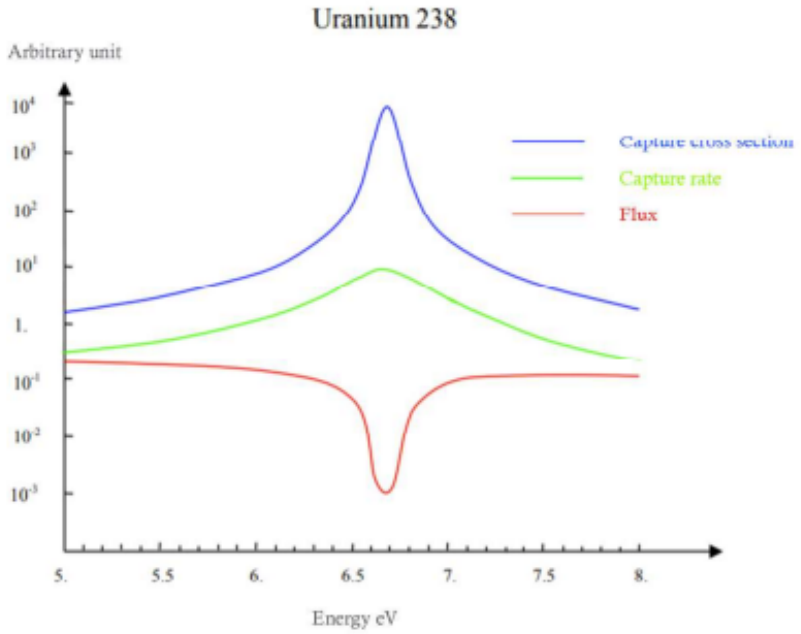

Figure 3.4: The self-shielding phenomenon[10].

3.2 Stochastic neutronics code: Monte Carlo methods

The Monte-Carlo method is a probabilistic approach, based on the study of the possible interactions to which neutrons are subjected during their lifetime. It is a method that does not directly solve the Boltzmann equation, as deterministic methods do, but instead simulates the neutron transport reaching at the evaluation of the quantities of interest, such as the neutron flux. In order to study all the possible event occurring during the life of a neutron, this technique is based on the random walks of these free particles; the method simulates and follow the trajectory of each neutrons from their birth, probably due to a fission event, until their death, due to absorption or leakage. It is possible consider this trajectory as a series of event that is called "history", which depends on the position, energy and direction of the particle, the distance between two consecutive events and the type of interaction. To obtain an accurate calculation of the physical quantities of interest, with a relatively low uncertainty, it is necessary to simulate a substantial number of series of neutron

events. This entails, on the one hand, an excellent precision of calculation, and on the other, a huge computational cost. For this reason, in the context of the study of neutron behaviour, codes based on the Monte-Carlo method are used for the steady-state calculations and, for the accuracy of the obtained precision, are currently the reference codes for the validation of simplified neutron calculation schemes.

3.3 Depletion solvers

In order to solve the Bateman equations, evaluating the concentration of isotopes as a function of time, it is possible to use different mathematical methods depending on the hypotheses considered. One of the best schemes to have an excellent compromise between accuracy of results and computational time is the Runge-Kutta method, of order 4 [10]. The general depletion equation can be written in matrix form as:

$$\frac{\mathrm{d}N_i}{\mathrm{d}t}(t) = S(t) + A(t)N(t) \tag{3.13}$$

Where:

- $N(t)$: vector of the concentrations of the considered nuclides
- $S(t)$: vector of the source term
- $A(t)$: generation/depletion matrix in which the diagonal elements contain the terms of nuclide disappearance due to decay and transmutation, and the non-diagonal elements contain the supplying term

The depletion matrix depends on the time because it depends on the flux, that is one of the results on the neutronic transport code; for this reason the various terms of the matrix can be known at any moment and in particular for each burn-up step. The Runge-Kutta scheme is based on Euler method and on the Taylor expansions at a precise and setted order of $N(t)$. It is possible to consider:

$$G(N) = S(t) + A(t)N(t) \tag{3.14}$$

The 4-order of Runge-Kutta scheme is:

$$\begin{aligned}
N^{(0)} &= N^{(n)} \\
N^{(1)} &= N^{(0)} + \frac{\Delta t}{2} G(N^{(0)}) \\
N^{(2)} &= N^{(0)} + \frac{\Delta t}{2} G(N^{(1)}) \\
N^{(3)} &= N^{(0)} + \Delta t G(N^{(2)}) \\
N^{(4)} &= \frac{\Delta t}{2} G(N^{(3)}) \\
N^{(n+1)} &= \frac{1}{3}(N^{(1)} - N^{(0)}) + \frac{2}{3}N^{(2)} + \frac{1}{3}N^{(3)} + \frac{1}{3}N^{(4)}
\end{aligned} \tag{3.15}$$

Where Δt is the time mesh interval. The error introduced by this calculation scheme is proportional to Δt^4.

Chapter 4

Context and neutronics tools used

4.1 Context and case study

The subject of the studied case is a small PWR (pressurized light water reactor) with a heavy reflector. It is a bench-marking case which allows to study the same fuel assembly characteristics of a standard light water reactor with a heavy reflector with a smaller scale and so a reduced computational cost.

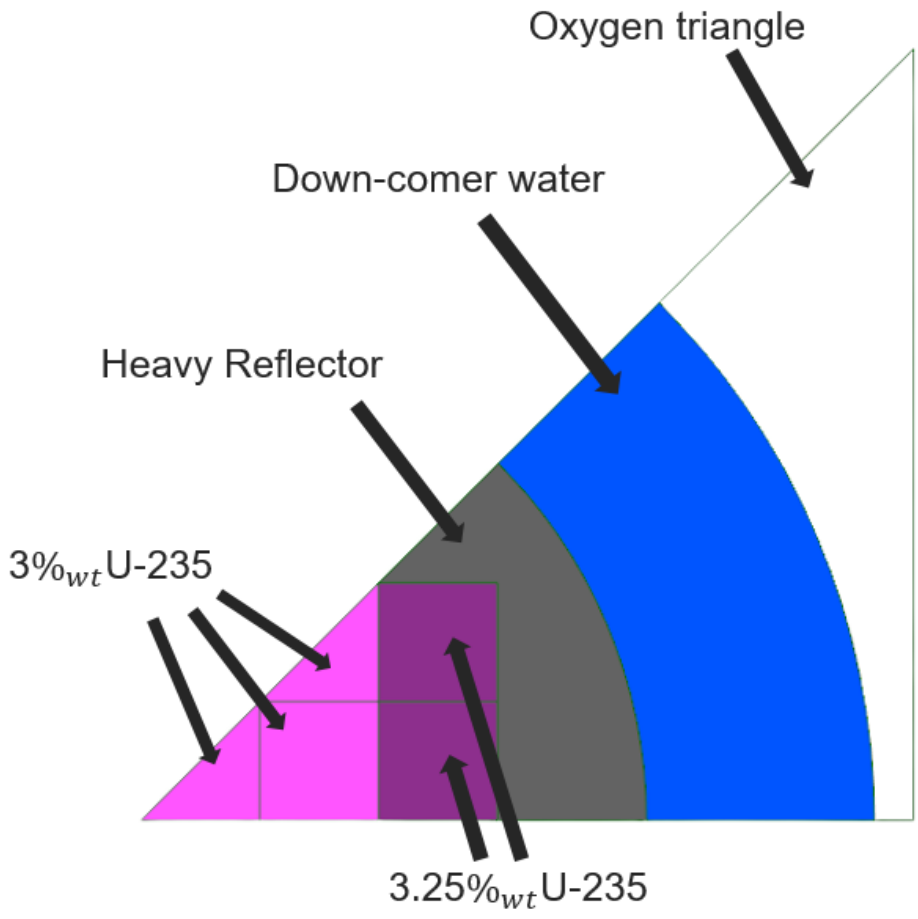

Figure 4.1: Schematic view of the core geometry.

The objective is the implementation of a generic and complete neutronic calculation scheme with depletion in 2-D using the lattice part of APOLLO3®, testing different methods for self-shielding calculations. The scheme for this setup studied here can be validated with reference results from Monte Carlo calculations (with TRIPOLI4®) [14] and deterministic calculations (with the former generation code APOLLO2) that are available. The use of standard industrial simplified schemes with APOLLO3® enables the calculation of the physical quantities of interest for the design and operation of nuclear reactor. The ideal validation of these schemes is with Monte Carlo code but it is constrained by large computational cost and limitations in depletion. Therefore, one of the way for the validation is to use a deterministic scheme on 2D cores based on MOC (Method Of Characteristics) with fine energetic mesh (SHEM281).
The core is composed by 32 assemblies. Each assembly is made by 17x17 cells of which 25 are guide tubes and 264 are fresh fuel pins. The fuel cell composition is low enrichment and with two different levels; 4x4 central assemblies contain cells with $3\%_{\text{wt}}$ of U-235 (the lighter ones in Figure 4.1), while the remaining peripherals contain cells with $3.25\%_{\text{wt}}$ of U-235 (the darker ones in Figure 4.1). The entire calculation is performed with all the control rods out (ARO) and the guide tubes are filled with water. To take into account the presence of the spacer grids, their isotopic concentrations are diluted in the water composition surrounding the various cells. Around the assemblies there is a water gap and then the reflector in which, like for the spacer grids, is diluted water to account the perforations filled with the latter. The reflector, in the end, is surrounded by down-comer water and an oxygen triangle (Figure 4.1). A better explanation is given in chapter 6 of this case study.
Thanks to the symmetry with which assemblies are arranged in the core, it is possible to study only one eighth of the entire geometry (Figure 4.1).
The isotopic composition of the moderator structural materials does not change during the depletion chain; the depleting compositions are exclusively those of the fuel pins because the structures do not have, in their composition, isotopes subject to depletion and the moderator is continuously renewed during the operational phase of the reactor.

4.2 APOLLO3®

4.2.1 Code presentation

APOLLO3® is the new multi-purpose deterministic nuclear code developed by the CEA, in partnership with Framatome and EDF. It can compute both water thermal reactors (like PWR) and fast reactors (like ASTRID). It includes all the functionalities of the previous generation codes such as APOLLO2, CRONOS2 and ERANOS incorporating both lattice calculation and full-core simulation tools [15].
The code structure is mainly based on object-oriented architecture written in C++ and FORTRAN 90, but there are three available user interface: a Python API (Application Programming Interface), a C++ API and a keyword/value-text based API. One of the advantage to have a Python interface is its versatility in utilizing various

functionalities, such as looping and modules, to enhance the performance of the input data set. The evaluation of the nuclear physical data utilized by APOLLO3® are provided by four external libraries that store nuclear cross-section, self-shielding data (in form of probability tables and reaction rate) and depletion data (in form of depletion chain). These libraries are produced by CEA's platform GALILEE, which exploits the JEFF-3.1.1 library to generate coherent data for all the CEA codes.
APOLLO3® is a modular code in which different procedures and sequences of operations are required in order to calculate the physical parameters of interest for a particular nuclear core.
For each task there is a specific module (materials definition, geometry construction, self-shielding evaluation, flux resolution) and and it is the user's task to combine them together to achieve the goal. The input and output of each module can be considered as an object (materials, geometry, cross-sections, flux), which can be used, in turn, in others procedural operations.
In order to solve the integral form of transport equation the code can use either the collision probability method or MOC (Method of Characteristics). In the next section is presented the method used for the studied case.
Concerning the depletion calculation, APOLLO3® is equipped of a module that allows the evolution of the core at different burn-up steps, without needing to use another code. At each step, knowing the reaction rate obtained by solving the transport equation, it evaluate the new concentration of each isotope and their cross-sections values for the different media present in core; this calculation is performed coupling all lattice and core solvers with the MENDEL-solver library, integrating the Bateman equation on the burn-up range with a Runge-Kutta fourth-order method.

4.2.2 Implemented calculation scheme

The calculation scheme developed, in general, is nothing more than a succession of the necessary steps, procedures and sequences of operations, to arrive at the calculation of the neutron flux and other quantities of interest [16] [17]. The structure of the lattice data-set for the preliminary and core cases that this work will introduce is presented in general way in Figure 4.2.
The input and starting point of the scheme is the acquisition of basic nuclear data in the CEAV5.1.2 library, which is based on data from JEFF-3.1.1 [18] and SHEM281 for neutron energy groups. The library is generated by the platform GALILEE to ensure consistency with the pointwise library created for TRIPOLI4®. SHEM281 is a fine energetic mesh (281 neutron energy groups) that is optimized to calculate UOX thermal reactors and it can minimize the error of the approximation. About the depletion, a file contains all the isotopic chains which contribute to this phenomenon and which must be taken into account.
The first real step to be implemented concerns the definition of isotopes and the construction of materials and geometries that will constitute the media of the system studied. The isotopes are linked to the libraries mentioned above that define data for cross-section and, for those needed, self-shielding.
Then all materials are defined, specifying the composition and therefore the isotopes of which they are formed and their concentration; for materials such as fuel,

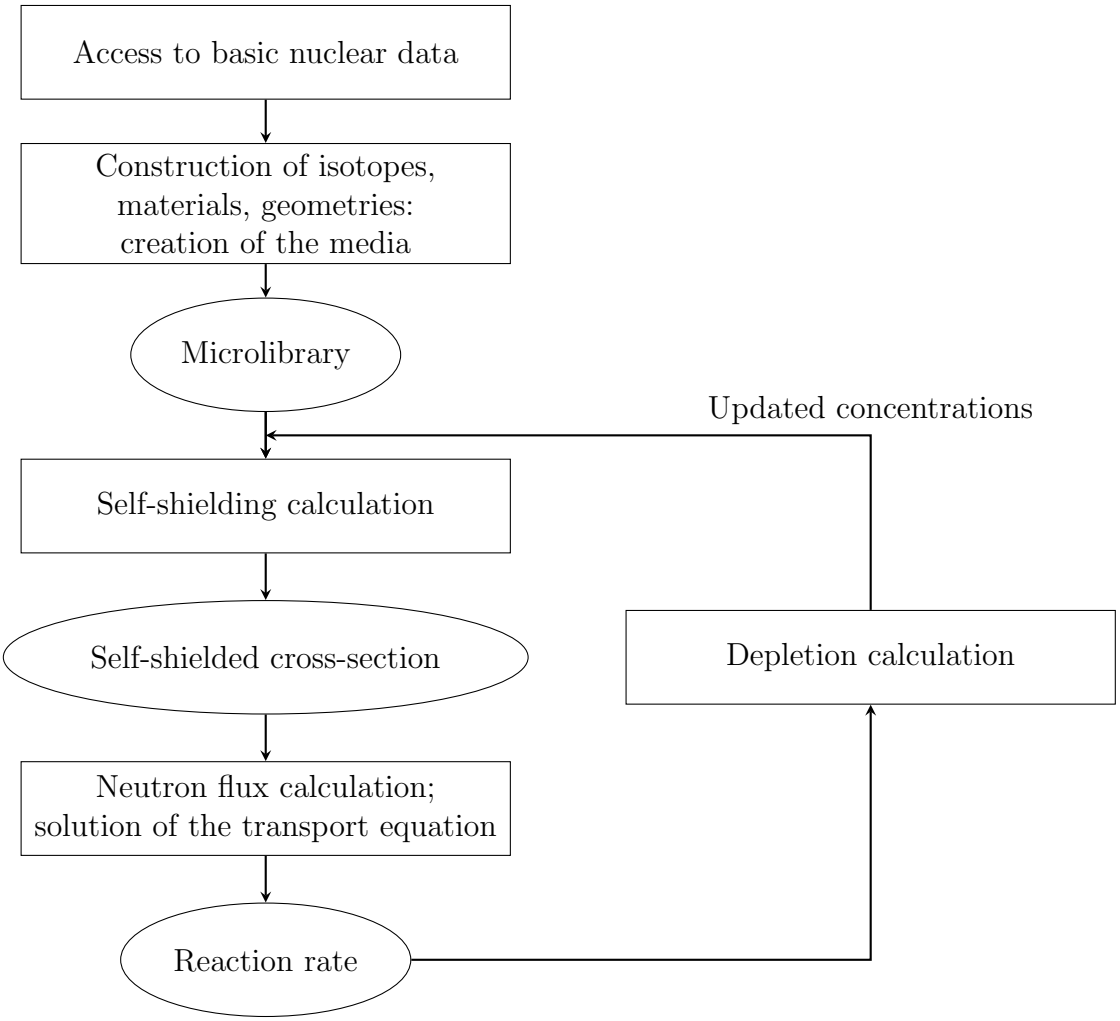

Figure 4.2: General flowchart of the calculation scheme.

the class used for depletion data is also specified, containing all isotopes used for the depletion calculation.
After this, the necessary geometries are initialized and constructed.
In APOLLO3® there are several types of classes to define the geometry, such as GeometryCell, GeometryCellRefined, GeometryGrid, GeometryGridRefined, according to what is being built.
In the cases studied, the first two classes were used for the construction of the geometry of the fuel cells and the guide tubes, respectively for the calculation of self-shielding and the calculation of the neutron flux (Figure 4.3). The mesh refinement is necessary to provide a good convergence of the neutron flux solution. The third class, instead, was used for the construction of the assembly and core geometry. There is also the possibility to import geometries from external tool ALAMOS.
Once the required geometries have been defined, it is possible to create an association between the latter and the materials, temperature and properties using a specific module in the code. In this way the media is created and placed in the geometry and, after defining boundary conditions, the mesh can be created for a

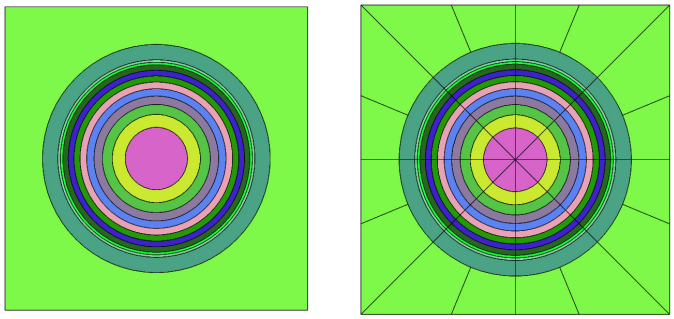

Figure 4.3: Example of cell geometry for self-shielding and flux calculation.

specific solver. At this point it is possible to proceed to the next step and generate the Microlibrary, libraries containing the microscopic cross-section of the isotopes present in the media. The fourth step is the calculation of the self-shielding from which are obtained the self-shielded macroscopic cross-sections, necessary for the next step concerns the calculation of the neutron flux. Now, only the solver options and solver initialization are missing. The discussion of the specific methods for the calculation of self-shielding and flux used in the calculation scheme implemented for the cases under examination will be the subject of the next section.
The reaction rates are obtained as a result of the transport solution and is used for the depletion calculation. By solving the Bateman equations with the Runge-Kutta method, the new isotopic concentration is evaluated and, at this point, it is possible to restart the calculation for the next burn-up step.
Before generating the output files, the results are homogenized to a simplified geometry and condensed in two energy groups, defining respectively the fast group and the thermal group, as shown in the Table 4.1.

Energy group number	Energy range [MeV]
1	$19.64033 - 6.25 \cdot 10^{-7}$
2	$6.25 \cdot 10^{-7} - 1.1 \cdot 10^{-10}$

Table 4.1: Energy groups for homogenization.

4.2.3 Calculation methods

During the development of the project, several solvers available in the code are used, in particular for the calculation of self-shielding. In fact, the TDT MOC SHEM-281 solver has always been utilized for neutron flux calculation with a set of parameters that accurately represent the system implemented. The MOC is performed with constant flux in each mesh of the geometry and a 3^{rd}-order of anisotropy. k_{eff} precision is set at 1 pcm on the last two outer iterations while fission integral tolerance is set to 10 pcm.

Regarding the angular discretization, 24 horizontal angles are used for the quadrature formula.
Instead, for the evaluation of the self-shielding various methods are tested, implementing the calculation not only on the entire geometry but also trying to solve it independently on each subdomain. With regard to the technique used, the calculation is always performed with a the fine-structure method (Livolant-Jeanpierre) but, about the solvers, it is possible to distinguish different cases, called as below:

- FULL EXACT (FE): the evaluation is performed on the entire geometry with TDT Pij solver;
- FULL MULTICELL (FM): the self-shielding is evaluated on the entire geometry with Multicell Pij solver;
- SUB EXACT (SE): the calculation is performed on subdomains with TDT Pij solver;
- SUB MULTICELL (SB): self-shielding calculation on subdomains with Multicell Pij;
- FLUXGROUPEMENT (FG): the evaluation is performed on subdomains with Multicell Pij, grouping similar cells.

The first is the reference case with the most correct self-shielding flux solution both because a method with a better approximation is used and because the calculation is performed on the whole geometry and not on parts of it independently. While this makes the solution more accurate, it also increases the computational time, especially for large and complex geometries. In addition, this last aspect is further accentuated for the subsequent steps of the depletion mesh; unlike the calculation of the k_{eff}, whose convergence becomes faster at each step, the evaluation of the self-shielding takes more and more time due to the presence of an increasing number of isotopes to be considered, produced during the operational phase of the reactor.
The other cases have been tested for the simple reason that, having a greater approximation, they have a lower computational cost; the significant aspect is to have a balanced compromise between the accuracy of the results and the calculation time, especially for very complex geometries and in depletion where time gain becomes significant. As will be shown in the following chapters, the case of greatest interest will be that of FLUXGROUPEMENT (FG), in which in addition to evaluating self-shielding independently on portions of the geometry and with a Multicell solver,cells with similar environment are grouped together. In this way the calculation is speeded up considerably because it is done only once for each group (if there are different groupings) and not for each cell that makes up the geometry.

4.2.4 Approaches adopted for the comparison

This section presents the methods used to compare the results between the different codes for the validation of the calculation scheme. The first, used for both steady-state and depletion, is the evaluation of reactivity discrepancy. The reactivity ρ is the deviation of the reactor from its critical state; it is a measure of departure from criticality. The reactivity is commonly expressed in *pcm* (per cent mille) and is defined as follow:

$$\rho = \frac{k_{\text{eff}} - 1}{k_{\text{eff}}} \cdot 10^5 \quad [pcm] \tag{4.1}$$

The discrepancies are evaluated by calculating the difference in reactivity values between the reference case and the one to be verified:

$$\Delta\rho = (\rho_{\text{calc}} - \rho_{\text{ref}}) = \left(\frac{1}{k_{\text{eff,ref}}} - \frac{1}{k_{\text{eff,calc}}} \right) \cdot 10^5 \quad [pcm] \tag{4.2}$$

Where:

- ρ_{ref}: reactivity of the reference case;
- ρ_{calc}: reactivity of the calculated case.

This method, even being a good global indicator, is not enough to confirm the good performance of the calculation scheme. For this reason, the other comparison performed is the evaluation of the reaction rate, and in particular the fission rate. The estimation of the relative percentage error is carried out with the formula:

$$\delta f^{i,j} = \frac{f^{i,j}_{\text{calc}} - f^{i,j}_{\text{ref}}}{f^{i,j}_{\text{ref}}} \cdot 10^2 \tag{4.3}$$

Where $f^{i,j}$ is the fission rate in a position i, j; each term, being already normalized, does not need to be divided by the average value.

4.3 The ALAMOS interface

ALAMOS is the new graphical user interface (GUI) specially developed for APOLLO3® as a module of the SALOME platform. It is used to build structured and unstructured geometry in 2-D and for numerical simulation. Compared to the previous generation code (Silène), ALAMOS offers, in addition to the graphical interface, the possibility of using a Python programming interface that allows the creation of simple scripts and advanced modules, making it easier to use even for the most complex geometries [19].
Typicaly, objects in ALAMOS are represented or described through layers. These layers encompass various aspects including geometry, material composition and addition information pertaining to their interactions with other objects. The ALAMOS data model is based upon the object layer which consists of a geometric structure, comprised of points and lines, and fields of property, temperatures and materials can be assigned. The data regarding the geometrical and physical aspects of the

structures are produced and stored as media files. These files are then referred to, in APOLLO3® data set, as unstructured geometry objects.
ALAMOS is employed as a essential tool in constructing the outer region of the core, playing a key role in refining the geometrical details. Notably, the reflector's mesh undergoes a automatic triangular refinement with an objective mesh size of 1.3 cm. The goal of the refinement is that each mesh has a maximum size of 1.3 cm. Simultaneously, the down-comer's mesh is characterized by an objective dimension of 3 cm. This approach to mesh refinement aligns with the intricate requirements of the core's external structure, facilitating a precise representation of its components while optimizing computational efficiency of the flux calculation.

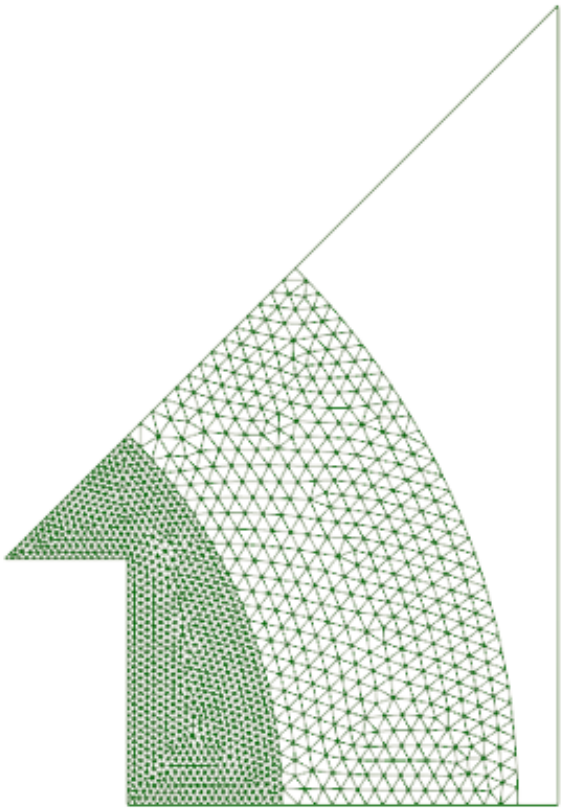

Figure 4.4: Ex-core unstructured geometry created in ALAMOS.

Chapter 5

Preliminary case study

In this chapter two preliminary cases will be presented, before moving on to the main case concerning the core of the small PWR. To set up APOLLO3® 2D core calculation scheme and so to learn the different steps to follow for the implementation, an incremental process is used. The study began by first treating a single cell and then a cluster composed of 3x3 cells, to move to a larger cluster composed of 3x3 of the previous clusters (called cluster 9x9 because it consists of 9x9 cells). After these cases, the discussion has passed to the study of a single assembly 17x17 to arrive in the end at the implementation of the entire core.
As anticipated, below will be treated only the last two preliminary cases, interesting for some aspects that will be discussed.

5.1 Cluster 9x9

The first interesting case presented is that of the cluster 9x9. This preliminary case is important because, during the implementation, there were interesting aspects regarding the use of the FLUXGROUPEMENT method, which certainly would have met also in the main case of the core. As mentioned above, the overall geometry of the cluster is composed of several geometric layers: it is composed of 3x3 smaller clusters (called sub-clusters), each of which is itself formed by 3x3 cells. The eight peripheral sub-clusters are composed of 8 cells with $3\%_{\mathrm{wt}}$ enriched fuel and the one in the center, which has in its concentration a certain amount of gadolinium. The central cluster is always formed by 8 normal fuel cells and the one in the center, instead of containing gadolinium, has in its place a guide tube. It is important to remember that the study is carried out in a situation with all control rods extracted (ARO) and therefore the guide tube is filled with water. Given the symmetry of the total geometry of the cluster, it is possible to study only one eighth, as shown in Figure 5.1, that displays the refined mesh for the neutron flux calculation.
The normal cells are divided into six zones, the first four are fuel rings while the last ring and the remaining part are occupied by cladding and water respectively. The cells containing gadolinium are divided into thirteen regions by twelve concentric rings; eleven of these are occupied by fuel, one by cladding, and the remaining part by water. The only guide tube instead is divided into three zones, progressively

occupied, from the inside to the outside, by water, cladding and water again. As mentioned in subsection 4.2.2, for the calculation of the neutron flux the cells are further refined and, for the present case, the rings are divided into eight sectors while the remaining part is portioned into sixteen sectors. Such refinement is proven to provide a good balance between the accuracy of the results and their computation cost. The intermediate sub-clusters and the final cluster have been constructed as grids with the specific APOLLO3® module. Under the assumption that the cluster is part of a system composed not only of one of them, and therefore is surrounded by other similar clusters and not by vacuum, the boundary conditions are required to be reflective.

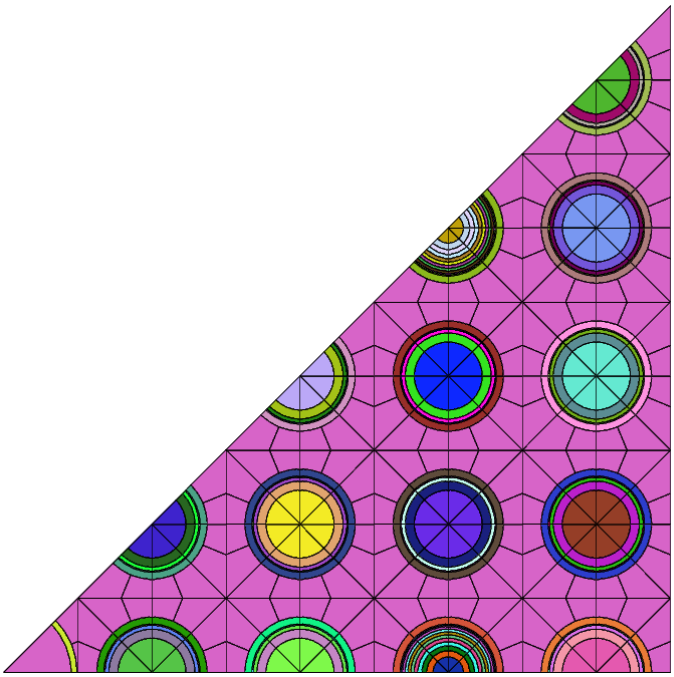

Figure 5.1: An eight cluster 9x9 meshing for the flux calculation.

The implemented and most interesting cases are the FE method, as mentioned above is the reference case, and the FG method. In particular, the focus will be on the latter case. To implement the FLUXGROUPEMENT method, as the first test, the intermediate sub-clusters are removed; in this way the cells are placed directly in the larger cluster, thus having no more three layers of overlapping geometries but rather two (cells and final cluster). The cells, with the exception of the only guide tube, are grouped in four groups: the cell adjacent to the guide tube and the one in the corner, alone constitute two different groups because they are the only ones that are close to a guide tube; the other normal fuel cells form another group and in the end, the cells with gadolinium constitute the additional and last group. With this method, self-shielding is evaluated over the entire geometry with the Multicell Pij solver. For this reason, this first case corresponds to FULL MULTICELL method with grouping. The correspondence between flux and self-shielding media is maintained and the discrepancy of k_{eff} values is relatively low, as will be shown in the following section.

The important aspect, however, is that the calculation is speeded up with a considerable gain in computational time compared to the reference method, as it is possible to see from the Table 5.1.

	FE	FM (with grouping)
Total SSH time [min]	38.11	4.77

Table 5.1: Comparison of total self-shielding time between FULL EXACT and FULL MULTICELL (with grouping) methods for the entire depletion mesh.

After this first test, a second case is implemented in which the FLUXGROUPEMENT method is applied on the starting geometry with intermediate sub-clusters. This time the cells are grouped within the subdomains and the calculation of self-shielding is performed for each of the intermediate clusters separately. For the central sub-cluster, containing the guide tube, as previously the two fuel cells form two different groups, because the difference in the position occupied means that they cannot be treated as similar cells (there is a huge difference between a cell on the side to a guide tube and one in the corner). For the remaining sub-clusters, all normal fuel cells constitute a group, leaving out the gadolinium cell.

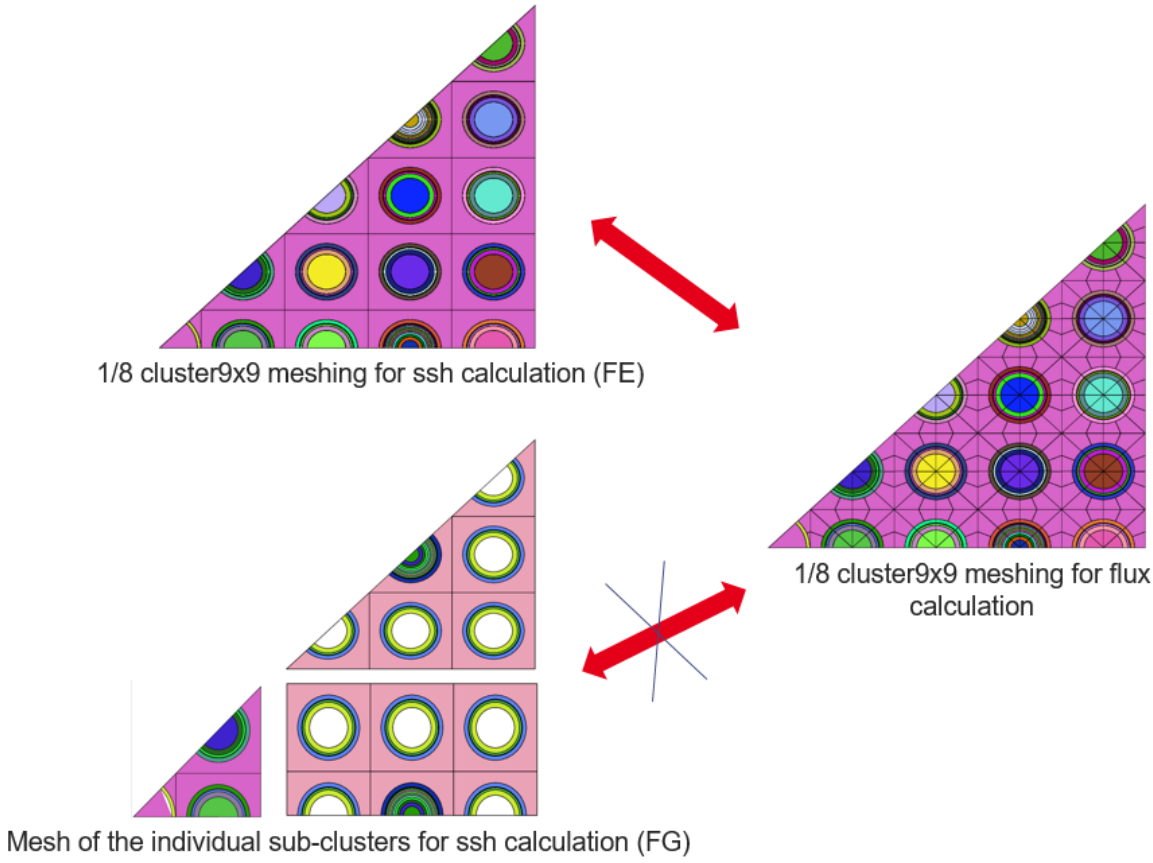

Figure 5.2: No link between the media of the self-shielding and the media of the flux in case of FG with sub-cluster.

In this case the link between the neutron flux media and the self-shielding media is lost, as it is possible to see in the Figure 5.2 (same color cells in meshes for ssh and flux calculation in case of FULL EXACT). The code, once the neutron flux has been calculated for the first step of the depletion mesh, is unable to automatically update the isotopic concentration of the various cells and zones within them for the calculation of the next depletion step. Therefore, the evaluation of self-shielding is always carried out using the starting concentration and this can lead to a not negligible error.

5.1.1 Implementation of the concentrations update methods

In order to create the link between the flux and the self-shielding, it is necessary to implement a scheme, consisting of various functions and steps to follow, able to manually update the concentration of isotopes in different areas in a correct manner. The flowchart below represents the general scheme used directly in the dataset to create the match.

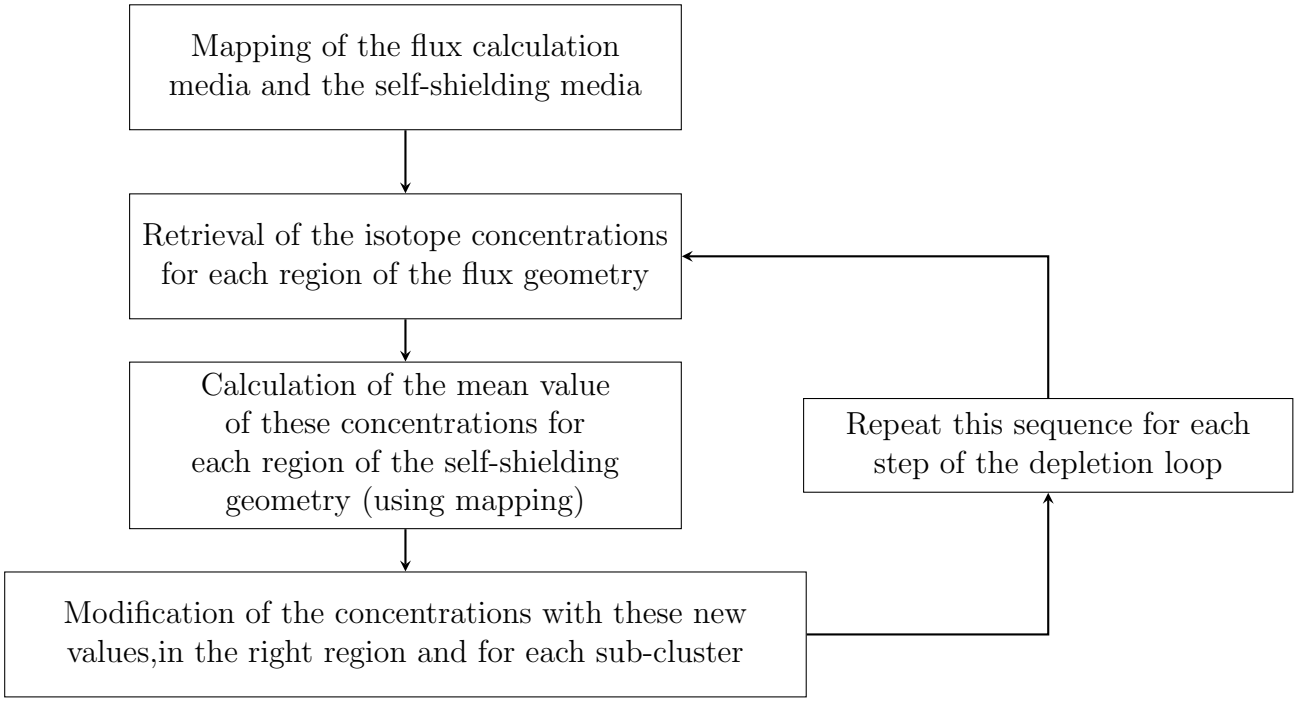

Figure 5.3: Scheme for manual isotopes concentrations updating.

The first step is to recognize, for each sub-cluster, which cells are grouped by mapping the media of the self-shielding and those of the flux; this is performed through the implementation of a function able to identify the cells grouped by the positions occupied in the geometry. After this, the next step is to retrieve the concentration for the different isotopes in each region of the flux geometry, and in particular for the different zones in which the grouped cells are divided (for the cell without

gadolinium the four fuel rings mentioned above). To evaluate the mean value of these concentrations, loops are implemented to manipulate these values for each of the mentioned regions and for each of the groups of cells present. To better understand it is possible to see the Figure 5.4, which shows the mesh for the calculation of self-shielding with the five cells grouped around the gadolinium one: the implemented functions recover the concentrations for each of the five cells in the flux media map and, for example, for the first inner zone (this operation is carried out for all regions); the mean value is calculated and projected in the corresponding zone, for all cells grouped, in the self-shielding media map.

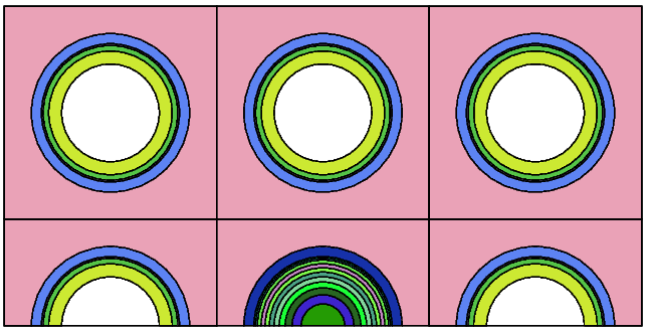

Figure 5.4: Example of cells grouping for a sub-cluster.

The insertion of the new concentration values is performed by another function. To make this update happen for all the depletion mesh, the different steps, from the second one onward, have to be put in practice in the depletion loop, so as to create manually the correspondence between flux and self-shielding. The different functions, implemented directly in the Python dataset, are written in the most general way so that they can also be used for other types of geometries without the user having to modify and adapt them.

5.1.2 Results and comparisons

This section shows the results of the various methods described. The comparison with the FULL EXACT reference case is done by evaluating the discrepancy of reactivity values in depletion through the formula shown in the subsection 4.2.4.
First, the performance of the FG case without the intermediate sub-clusters is evaluated; it can be noted that through the use of this approximate method, the calculation time of self-shielding is considerably reduced, very important aspect especially when talking about very large geometries as in the next sections about the other cases. As shown in Figure 5.5, despite the largest approximation, the discrepancy between this method and the reference one is around 10 pcm. Therefore, the quality of the result is not deteriorated but at the same moment, the computational time is decreased by 87.5% (see Table 5.1).
The graph of the Figure 5.6 shows the discrepancies between the reactivity values for the FE and for the case considering the presence of intermediate sub-clusters, in the event that the correspondence between the media of the flux and those of the self-shielding is lost and the one in which the match, created manually, is present and

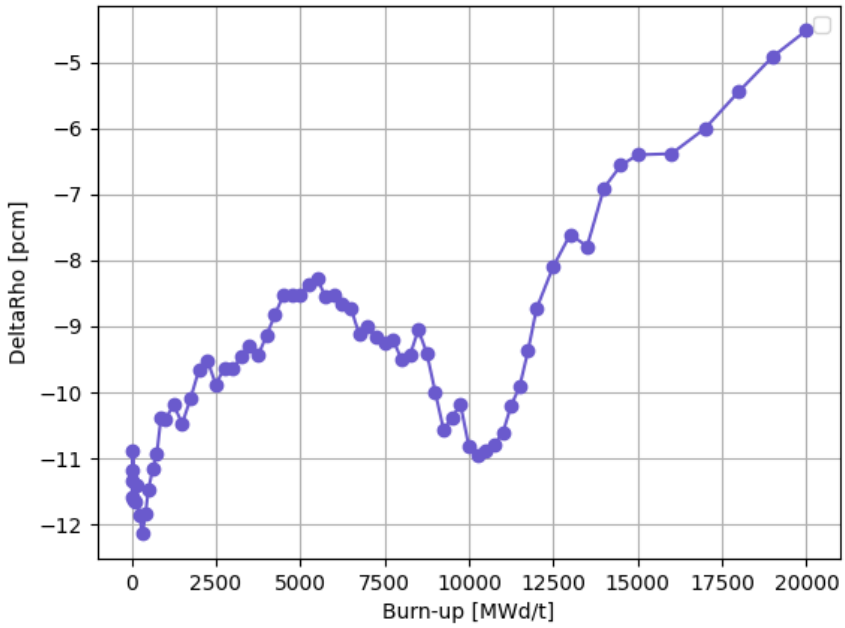

Figure 5.5: Reactivity discrepancies between FE and FG without intermediate sub-cluster.

consequently the concentrations of the various isotopes are updated. It is possible to notice that in both graphs, for the first point (burn-up = 0), the value of $\Delta\rho$ is the same. This is due to the fact that, ate the beginning, the isotopes concentration used is the correct one and specified by the user; the discrepancies value is about 12 pcm and it comes out from the use of two different methods, one with greater approximation than the other.
In addition, it is possible to observe that, in the case the updating functions are not improved, the discrepancy value reaches over 50 pcm, while in the case the match is manually created, the discrepancy is not so high and the trend of the curve is similar to the previous case without the intermediate sub-cluster. This is a sign that the implementation is correct and that, also in this case, the FLUXGROUPEMENT method works wells, leading to a good balance between result accuracy and calculation time.
In order to demonstrate the correct behaviour of the functions implemented, the difference in the concentration values, between the case with update and the one without, of the main isotopes during depletion is shown in Figure 5.7. The graph displays only concentrations whose relative difference exceeds, at least in one point, an imposed threshold value of 0.010 and only those concentrations with a value greater than 10^{-5}. It can be seen how uranium is consumed during the operational phase and also how other isotopes, in particular fission products, are created.

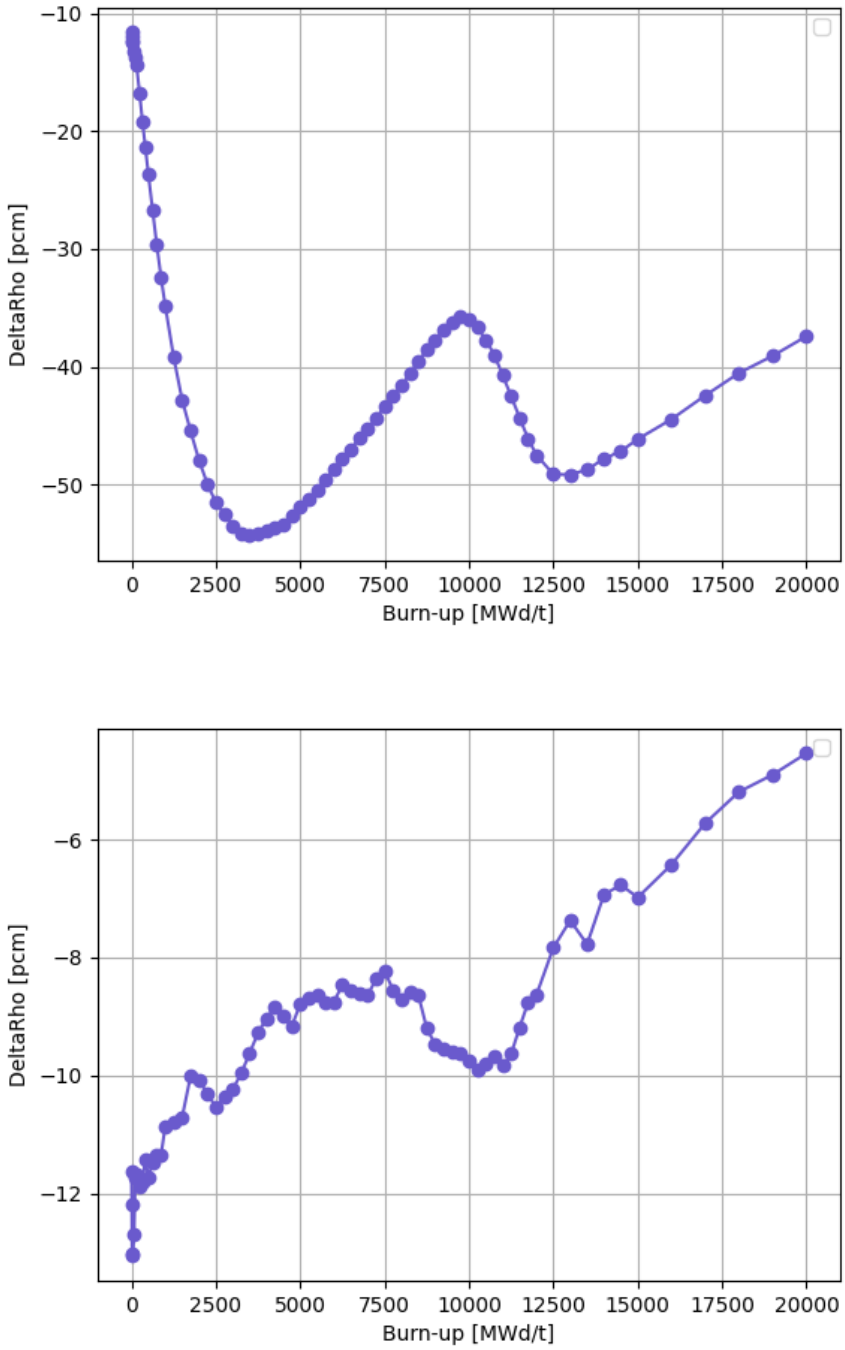

Figure 5.6: Reactivity discrepancies between FE and FG, in case without updating (top) and with (bottom).

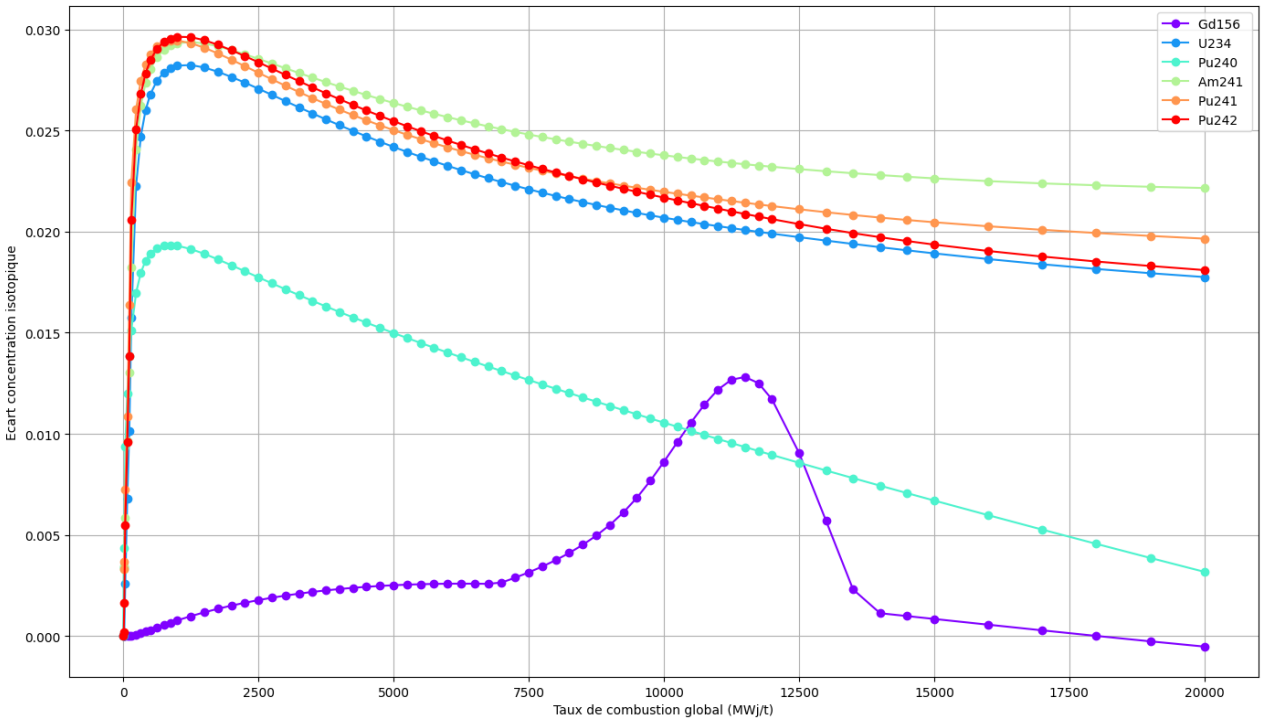

Figure 5.7: Concentrations discrepancies for main isotopes.

5.2 Assembly 17x17

The second preliminary case concerns the study conducted on the assembly 17x17, component of the core. The implementation of this case was fundamental to test the calculation scheme on a larger geometry and part of the final geometry of the whole core. The study of the assembly allows a quick verification of the performance to correct any discrepancies at a preliminary stage. In fact, for the first time, the results are validated through a comparison with those of APOLLO2.
The system consists of 289 cells, of which 25 are guide tubes and 264 are fresh fuel pins. Since in the core there are assemblies with different enrichment, during the implementation of the case in question in this section two different compositions of the fuel are defined, one enriched with $3\%_{\text{wt}}$ and one with $3.25\%_{\text{wt}}$ of U235. In this way for both types of fuel the calculation is performed and the results are verified.

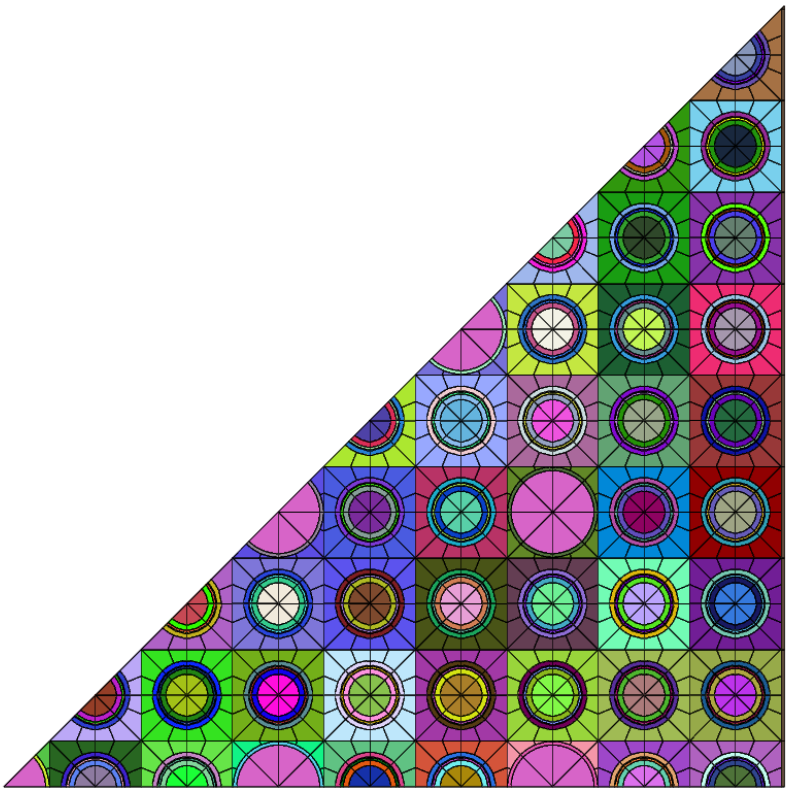

Figure 5.8: An eight fuel assembly 17x17 meshing for flux calculation.

As for the previous preliminary case, also here only one eighth of the geometry is considered, always for symmetry reasons (Figure 5.8).
The cells are always constructed in the same way; they are divided into six regions of which the first four are occupied by fuel, the next by cladding and the remaining part by water. The cells containing guide tube are divide into three zones such as the cluster 9x9. Also in this case, for the calculation of the neutron flux they are refined and the fuel and cladding rings are divided into eight sectors while the part occupied by water in sixteen sectors. Between the various cells there are spacer grids with the

function of ensuring the correct position of the pins inside the assembly. To take into account its presence, its isotopic concentration is diluted in the composition of the water surrounding the cells. For this reason, regarding the guide tube, two different compositions for water are defined inside the tube (remember that the calculation is performed in ARO) and outside the tube. Finally, around the assembly there is a strip of water built as a set of rectangular homogeneous cells for the reason that the Multicell solver needs a geometry of this type. Concerning to the boundary conditions, the assembly is only one of many that constitute the geometry of the core and to take this into account, therefore making the results more reliable, the so-called reflective conditions are considered.
For this geometry, the tested and implemented case are always the FULL EXACT (FE) and the FLUXGROUPEMENT (FG), just to have a first verification and to check the evaluation of the self-shielding of what will be the subdomains of the core. In fact, the FLUXGROUPEMENT method performed for the assembly is a FULL MULTICELL method (the self-shielding is evaluated on the entire geometry) with grouping similar cells and is useful to highlight the good performance in view of the core study, where the assembly is one of the subdomains on which the calculation of self-shielding is carried-out with this method. In this context, the fuel cells are grouped in five groups while the guide tubes constitute another single group.
A more detailed explanation is given in the chapter 6.

5.2.1 Results

This section presents the results for the fuel assembly in comparison with those of APOLLO2. Before evaluating the scheme in the depletion calculation, steady-state results are compared (burn-up = 0). This allowed quick verification of APOLLO3® scheme performance and to correct the discrepancies at the early stage of the study.

Enrichment	APOLLO2	APOLLO3®	$\Delta\rho$ [pcm]
3.00%	1.24502	1.24529	17
3.25%	1.26529	1.26555	16

Table 5.2: Full assembly k_{eff} calculation on burn-up zero.

The Table 5.2 shows the k_{eff} values for both the different fuel enrichment performed with the FULL EXACT method. It is also reported the discrepancies respect the results of the former generation code; the small reactivity deviation differences allow to deduce the good relation between the two codes in steady-state calculations. To guarantee the successful performance of the scheme, validation in depletion is conducted.
In this project, the initial fuel composition comprises a limited number of isotopes, including uranium, plutonium, and oxygen. This indicates that all the assemblies are at the Beginning of Life (BOL) stage, without any prior depletion.
This specific configuration is referred to as 'the first core', as it has not undergone

any shuffling or reloading of fuel assemblies.
The Figure 5.9 illustrates the reactivity differences between APOLLO2 and APOLLO3®, for FULL EXACT (in blue) and FLUXGROUPEMENT (in red), during the depletion of a single assembly. Only the results for the fuel assembly with 3.25%$_{\text{wt}}$ of U-235 are shown. Throughout the depletion process, the reactivity discrepancies in both cases remain below 30 pcm. The same behavior is also verified for the assembly with 3.00%$_{\text{wt}}$.
The relatively low values of discrepancy indicate that the good correlation between APOLLO2 and APOLLO3® is preserved even during depletion, providing confidence in the accuracy of both codes' predictions.

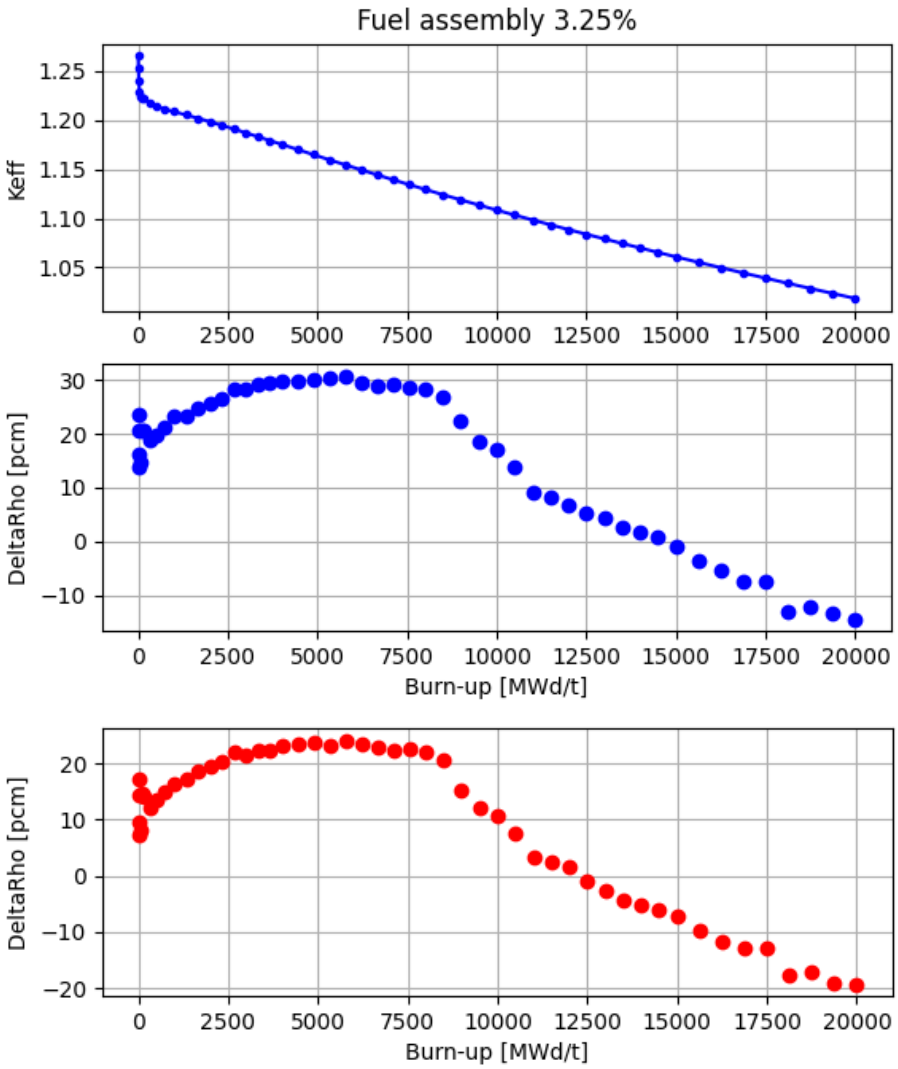

Figure 5.9: k_{eff} changes (top) and reactivity discrepancies (bottom) in the course of depletion. In blue the discrepancies of FE and in red that of FG method.

In the context of scheme validation, also a comparison of fission rates in depletion for the reference method (FE) is conducted between the two codes. The Figure 5.10

illustrates the results for the first burnup step of 9.375 MWd/t. As previously mentioned, to reduce computational effort, only a portion of the geometry is calculated due to its symmetry. The cells aligned along the symmetry lines are fully modeled instead of being halved. The energy spectrum is simplified into 2 groups (see Table 4.1).
The graph shows that the assembly exhibits the highest fission rates at its center, while lower values are observed in the periphery. This is expected, especially for a cluster without control rods that absorb neutrons and locally influence fission rates. The Figure 5.11 displays the fission rate discrepancies for each cell of the assembly between the two compared codes. The errors are presented as a percentage of APOLLO2's fission rates. The most significant absolute discrepancies occur in the area of highest fission rates in the APOLLO3® calculation. However, the maximum absolute discrepancy is only 0.11% and the average value is 0.067%, which are considered acceptable.

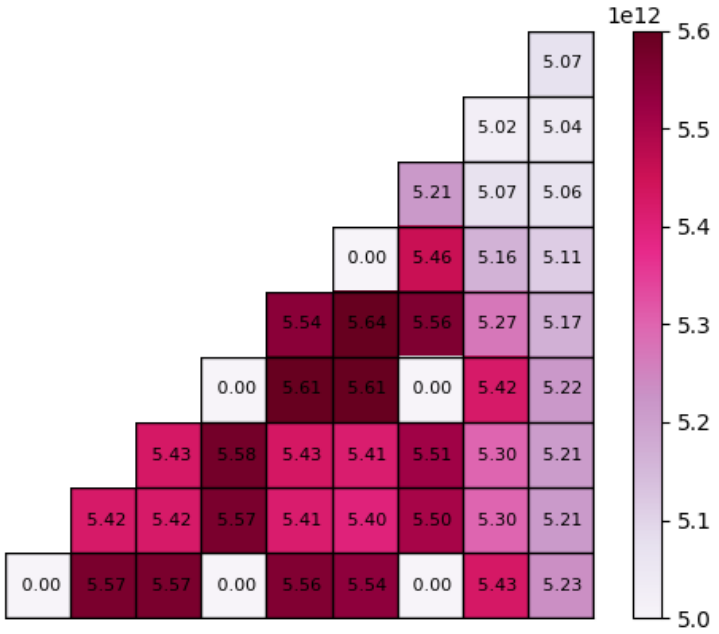

Figure 5.10: Fission rate of an eight of fuel assembly at the burn-up 9.375 MWd/t (in s^{-1}).

In addition, to give a global idea of how the fission rate discrepancy varies throughout the depletion chain, Figure 5.12 shows the trend of the standard deviation of the relative error percentage of each zone of the geometry with respect to its mean value on the whole pattern. From this graph it is evident how the deviation increases during the operational phase of the reactor, implying that the values tend to be less close to the mean value.

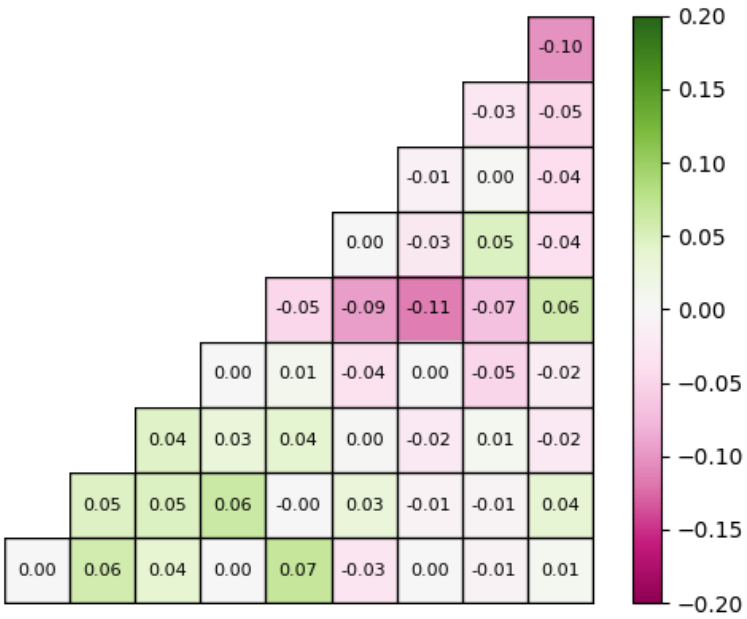

Figure 5.11: Fission rate discrepancies of an eight of fuel assembly at the burn-up 9.375 MWd/t (in %).

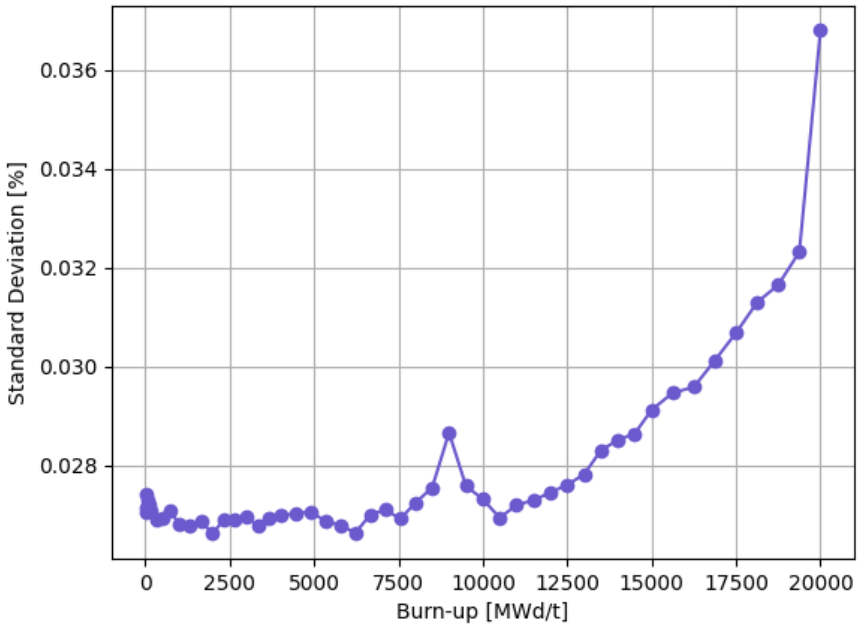

Figure 5.12: Standard deviation of the fission rate relative error between APOLLO3® and APOLLO2 (in %).

Chapter 6

Core case study

In this chapter is presented the main case study about the core of the small PWR with a heavy reflector. The first part is dedicated to the description of the geometry and how it is constructed, explaining why the inner part is built in APOLLO3® while the outer part concerning the reflector and water layer is built in ALAMOS. After this are presented the various methods implemented and the related results obtained, both in steady state and in depletion, also comparing them with those collected by APOLLO2 and TRIPOLI4®.

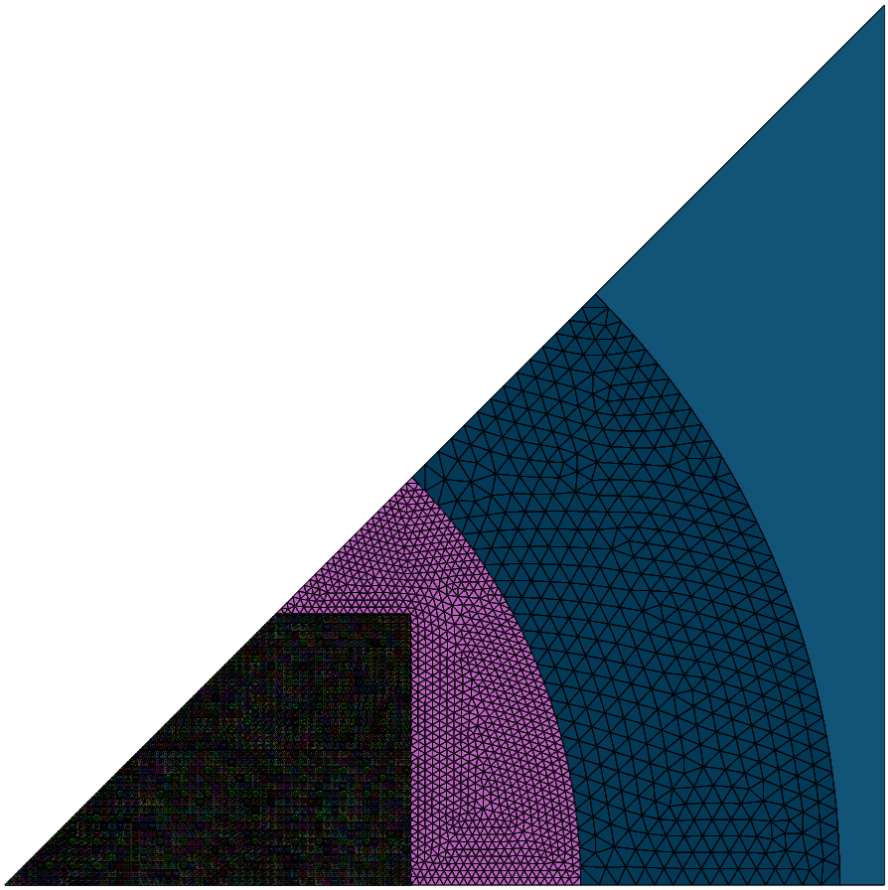

Figure 6.1: An eight core meshing for flux calculation.

The core is made up of 32 assemblies, each containing a grid of 17x17 cells. Among these cells, 25 are guide tubes, while 264 are fresh fuel pins. The fuel cells have low enrichment and are categorized into two levels: the central 4x4 assemblies have cells with $3\%_{\text{wt}}$ U-235, while the remaining peripheral assemblies contain cells with $3.25\%_{\text{wt}}$ U-235. During the calculation, all control rods are withdrawn (ARO), and the guide tubes are filled with water.
In each assembly is present a spacer grid with the function to hold in place the various cells. It is not really built so to take into account its presence, its isotopic concentration is diluted within the surrounding water composition.
Around the assemblies, there is a water gap, followed by the reflector. Lastly, this region is enclosed by down-comer water and an oxygen triangle (Figure 6.1). The outer part of the core is constructed using ALAMOS tool, because in APOLLO3® it is not possible to generate unstructured geometries, such as the studied reflector, but it is possible to import them from external files. On the other hand, the assemblies are designed directly in APOLLO3® because the Multicell calculation, in the case of serial self-shielding calculation on subdomains, is allowed only on structured geometries. Subsequently, the different pieces are joined together directly in the data-set. The core is built in the form of a grid, utilizing APOLLO3®'s dedicated module, with dimensions of 6.5x6.5 times the assembly's pitch.

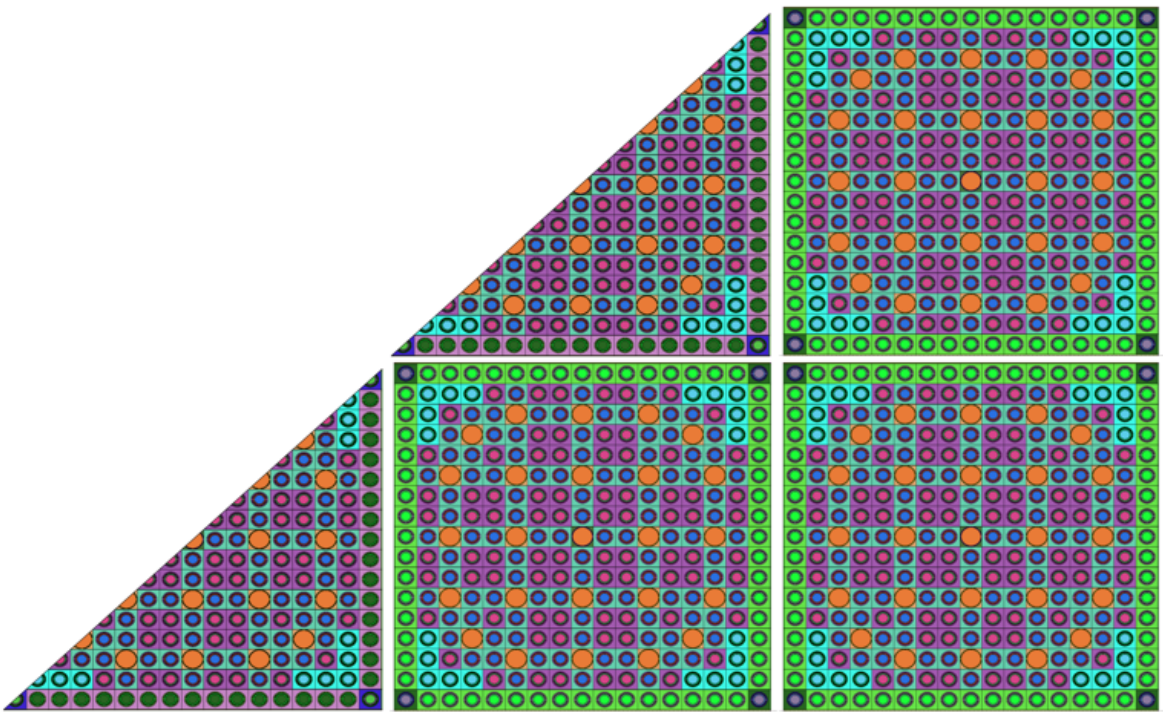

Figure 6.2: Assemblies meshing for self-shielding calculation (FG).

This design preserves symmetry and enables a focused examination of one-eighth of the complete core geometry. The assemblies are positioned as depicted in the Figure 6.1 (see also Figure 4.1), while the remaining regions are allocated to the geometry of the reflector, which is imported from ALAMOS.

This integrated approach allows for accurate representation of the core's spatial arrangement and its interaction with the reflector, contributing to a comprehensive understanding of the reactor's behavior.
To address the boundary conditions at the rear of the radial dimension of the reactor, a thin-oxygen triangle is employed. This choice is made because direct assignment to the reactor's curve is not yet supported in APOLLO3®.
In this case study, the nuclear core is analyzed using three different calculation methods: FULL EXACT, SUB EXACT, and FLUXGROUPEMENT. Each method offers distinct advantages and is employed to evaluate various aspects of the core's behavior.
The FE method, the less simplified and reference case, is used to perform detailed calculations by evaluating the self-shielding on the whole geometry.
Regarding the other two methods, they execute the calculation of self-shielding in series, independently for each assembly, targeting specific regions containing resonant isotopes. These regions encompassed all fuel assemblies and their water strips, as well as the steel reflector. Specially, for the latter it should be noted that to perform the calculation of self-shielding, it is necessary to reduce its structure to a 1D geometry, including part of the fuel to ensure the presence of a neutron source, otherwise the calculation would not be possible.
In principle, the computation load, measured by the number of Pij elements, escalates proportionally to the square of the cell number.
Thus, performing calculations for five fuel assemblies in a single universe is approximately 5^2 times more resource-intensive than executing each assembly individually in a sequential manner.
The difference between the two serial approaches lies in the fact that with the FLUXGROUPEMENT method the similar cells are grouped together and in this way the calculation is speeded up because carried out only once for each grouping.
In particular, as already mentioned in the previous chapter, for each assembly the the fuel cells are gathered into 5 different groups according to their position and arrangements.
The first group comprises cells located adjacent to the guide tubes. The second group includes cells positioned at the corner of the guide tubes. The third group consists of cells situated in the four corners of the assembly. The fourth group contains cells aligned along the sides of the assembly. Finally, the fifth group is formed by cells that create a kind of "L" shape near the corners of the assembly. The distinct grouping of cells can be easily identified and observed in the Figure 6.2.
As for the preceding cases, the standard cells are structured as follows: six zones are delineated, with the initial four zones forming the fuel rings, and the concluding ring and the residual section accommodating cladding and water, respectively. Similarly, the guide tube undergoes a division into three zones: from interior to exterior, these house water, cladding and water again.
In the context of neutron flux calculation, these cells experience an additional refinement. In the current instance, the rings are partitioned into eight sectors, while the remaining section is further divided into sixteen sectors. This refinement approach consistently demonstrates a ideal balanced equilibrium between result precision and computational efficiency.

6.1 Steady-state results

The core calculation involves a slightly different fuel composition compared to the assembly case, while the enrichment and calculation methods remain consistent in both scenarios. Initially, the computations encompassed self-shielding performed on the entire geometry. Although this approach guarantees accuracy and correctness in applying self-shielding, it also incurs excessively high computational costs. To address this, the next calculation models, the SUB EXACT (SE) and the FLUXGROUPEMENT (FG), introduced a serial approach for self-shielding, focusing only on regions containing resonant isotopes.
The advantage of the serial calculation lies not only in eliminating regions without self-shielded isotopes but also in significantly reducing the computational time, in particular for FG method in which the similar cells are grouped together. However, it is essential to recognize that self-shielding performed independently on parts of the geometry represents an approximation of the core environment.
Isolating each assembly from the surroundings and employing an infinite medium approach is less accurate than conducting self-shielding on the full core. This work explores the impact of this approximation on the results, particularly during fuel depletion. A comparison with the APOLLO2 results presented in Table 6.1 highlights the k_{eff} and timing for FULL EXACT reference case and for the serial calculation methods of SE and FG.

	APOLLO2	FE	SE	FG
k_{eff}	1.18943	1.18952	1.18948	1.18949
$\Delta\rho$ [pcm]	–	9	5	6
Total SSH time [min]	–	149	13	< 1

Table 6.1: Comparison core k_{eff} calculation on burn-up zero between APOLLO2 results and those of the different methods used in APOLLO3®.

It is evident that implementing self-shielding in series on selected parts of the geometry does not lead to a deterioration in the quality of results. On the contrary, this approach significantly reduces the computation time. This substantial reduction in computational requirements allows for faster and more efficient neutronic calculations, making the serial calculation of self-shielding a highly advantageous optimization. The core analysis benefits from the improved computational efficiency without compromising the accuracy of the results, highlighting the effectiveness of this approach for the considered nuclear reactor system.
To ensure the scheme's optimal performance, a more comprehensive analysis is conducted, focusing on fission rates calculation. Figure 6.3 displays the heat map of fission rates for one-eighth of the core, calculated using APOLLO3® FULL EXACT method. These results are presented only for this case because also for the other two methods of SUB EXACT and FLUXGROUPEMENT the behavior is the same. In this simulation, the diagonal fuel cells are fully modeled without being cut in half.

The energy groups were collapsed into two, as shown in Table 4.1. The average fission rate yields approximately 3.96 E+12 fissions per second. The highest reaction rate occurs in the center of the core, while the lowest is observed in the periphery, which aligns with the expected behavior for this geometry at zero burnup.

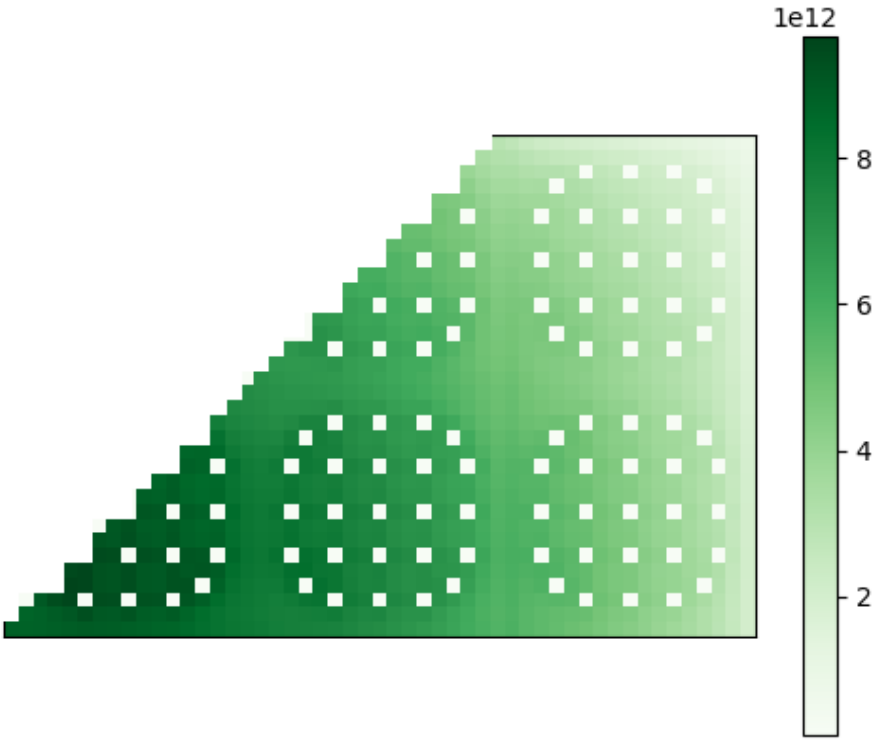

Figure 6.3: Fission rate of an eight of core at the burn-up 0 MWd/t (in s^{-1}).

The relative error values range covers from 1.24% to -9.08%, with the mean absolute value being 1.12%. A notable observation is the precise localization of the highest discrepancies, which are concentrated near the reflector. This region serves as the interface between two major elements of the geometry and undergoes a substantial flux gradient. The reason for these discrepancies could be attributed to the reflective boundary conditions applied to the geometry instead of using a void boundary.
The area with the highest discrepancies covers only a very small portion of the geometry, representing the lowest fission rates in the core. As a result, the absolute difference in fission rates is not very large and is considered acceptable. Despite the localized discrepancies, the overall agreement between the calculated fission rates of APOLLO3® and the reference values remains satisfactory, affirming the reliability and accuracy of the scheme's performance.

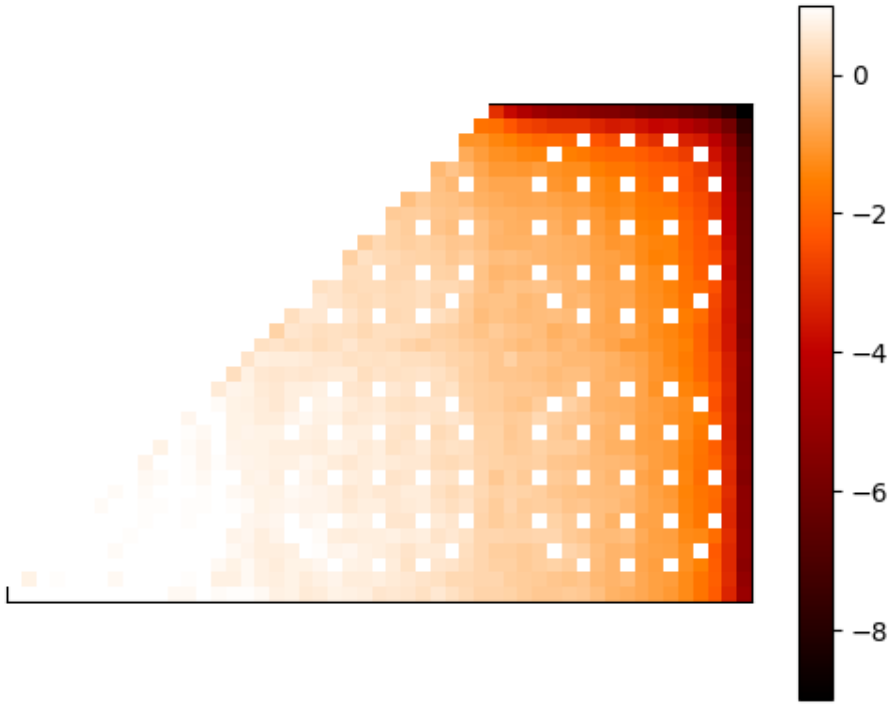

Figure 6.4: Fission rate discrepancies of an eight of core between APOLLO3® and APOLLO2 at the burn-up 0 MWd/t (in %).

6.2 Depletion calculation

In the context of calculating the evolution of the neutron flux for the core during depletion, the FLUXGROUPEMENT method emerges as the most practical and efficient approach. While the FULL EXACT and SUB EXACT methods offer high precision, their computationally demanding nature becomes increasingly burdensome as self-shielding calculations become more protracted with each depletion step.
In particular, although the SB method may show relatively lower computation times compared to the FE method for the initial zero burn-up step, it also proves impractical and impossible to utilize for large-scale depletion analyses. As the burn-up increases, the computational time for the SUB EXACT method quickly escalates, rendering it unfeasible for the comprehensive analysis of neutron flux evolution and its impact on the core during extended depletion periods. As a result, employing these methods for large-scale depletion simulations can lead to exorbitant computational costs.
In contrast, the FLUXGROUPEMENT method strikes a well-balanced compromise between accuracy and computational efficiency. By grouping similar cells together, this method effectively reduces the complexity of the calculations, making it more manageable for depletion analyses. While it involves a certain level of approximation, the FG retains satisfactory accuracy, allowing for reliable insights into the core's behavior over time.

Therefore, for practical and time-sensitive depletion studies of the nuclear core, this last method remains the preferred choice. Its ability to deliver reasonably accurate results while significantly reducing computational overhead makes it an indispensable tool for understanding the dynamic neutron flux evolution and its impact on reactor performance during depletion.
During the core's depletion analysis, a notable aspect is the treatment of self-shielding calculations concerning plutonium isotopes. Specifically, only the Pu239 isotope is considered, omitting the other isotopes that, although less prominent, could potentially influence the self-shielding effects.

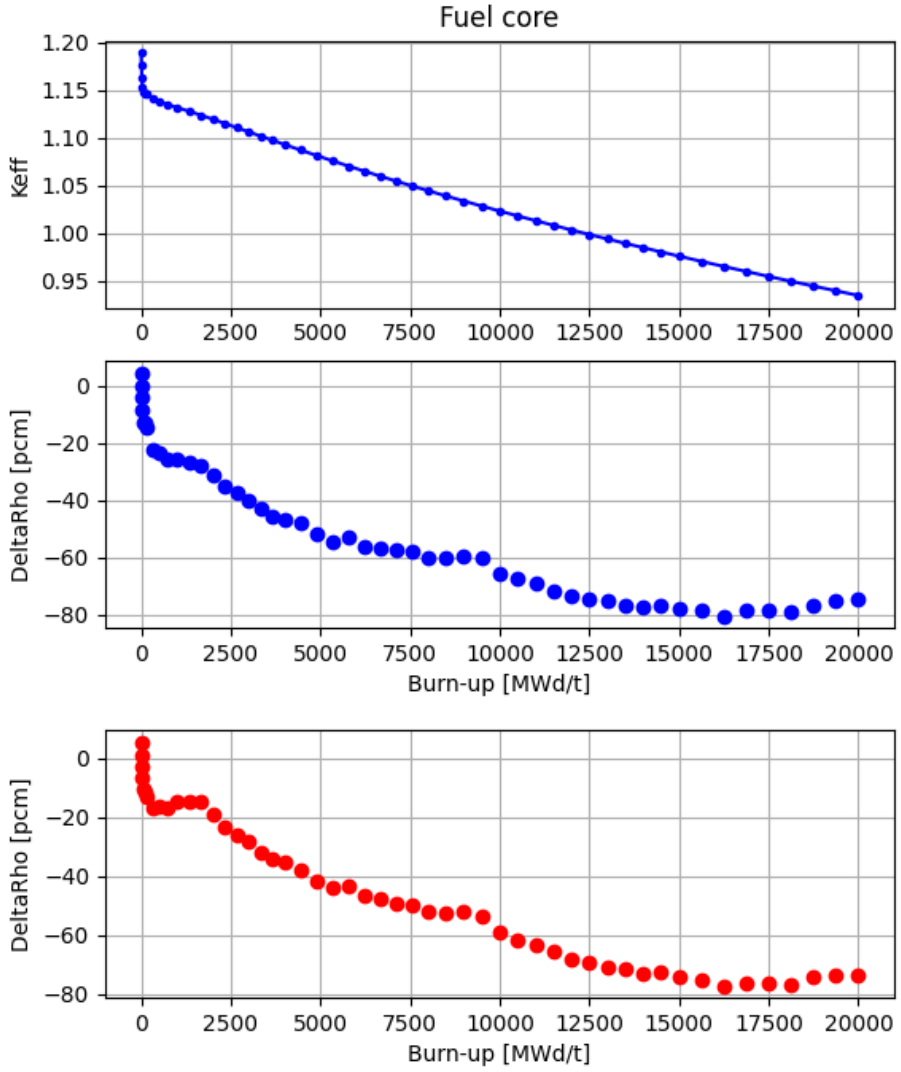

Figure 6.5: k_{eff} changes (top) and reactivity discrepancies (bottom) in the course of depletion. In blue the discrepancies of FG without updating and in red that of FG with updating.

This selective approach is adopted due to practical considerations. Inclusion of all plutonium isotopes in the self-shielding calculation caused the simulation to crash

after just a few burn-up steps, resulting in a segmentation error.
The investigation of the preliminary cluster 9x9 case holds predominant significance, as it revealed a crucial insight. This underscores that, grouping the similar cells in each subdomain, the direct link between the flux and self-shielding media is compromised.
In the context of the examined core, a similar scenario of three overlapping geometries (cell, assembly, and core) is present. This similarity highlights the need to address the potential loss of the link observed in the previous case. To mitigate this, it becomes imperative to incorporate the same set of functions utilized before to create manually the match and therefore to ensure the correct isotopic concentration updating.
The initial stage involves identifying the cells grouped within each assembly by mapping the media of self-shielding with those of the neutron flux. This is achieved through the integration of a function capable of discerning cells grouped based on their respective positions in the geometry.
Following this identification, the focus shifts to retrieving the isotopic concentrations within each region of the neutron flux geometry, particularly in the distinct zones that encompass the grouped cells.
Calculating the mean concentrations necessitates the implementation of loops to manipulate these values for each of the aforementioned regions and the various groups of cells within an assembly. The insertion of the new concentration values is executed through a separate function. This process ensures the establishment of a manual correspondence between the neutron flux and self-shielding effects for all stages of depletion.
Both scenarios, one with the implementation of these correspondence-establishing functions and the other without, were thoroughly examined. As observed from the graph of Figure 6.5, in contrast to the preliminary case involving the 9x9 cluster, the discrepancies of each method in comparison to APOLLO2 are nearly equivalent. The values do not exceed 80 pcm during depletion and there is a difference of less than 10 pcm between the two cases.
This minimal discrepancy between the two is likely attributed to the core's homogeneity. In contrast to the preliminary case, the absence of gadolinium cells in this instance suggests that it might have had a more pronounced influence on the self-shielding calculations. The gadolinium is entirely consumed over the course of depletion, thus necessitating the constant update of its concentration and, subsequently, the cross-section values in the depletion calculation.
This dynamic behavior is of substantial importance to accurately capture the evolving nuclear reactions. However, in the current core scenario where gadolinium is absent, as evident from the graphs, performing self-shielding calculations using the initial concentrations and, consequently, the same cross-sections, doesn't lead to a significant discrepancy.
This insight highlights the complexity of self-shielding calculations, underscoring how certain isotopes can wield varying degrees of influence depending on the core's specific composition and arrangement.
An additional exploration within the depletion analysis involved conducting calculations without refining the geometry for neutron flux calculations.

As evident from the graph, this approach resulted in a substantial discrepancy in reactivity, exceeding 200 pcm and nearly reaching 300 pcm.
Although adopting this method led to a faster computation process, it also produced notably inaccurate results.
This observation underscores the critical importance of geometry refinement.
While computational efficiency is crucial, it should not come at the cost of compromising result precision, particularly in complex nuclear core simulations where minute changes can exert significant impact on the overall behavior of the system.

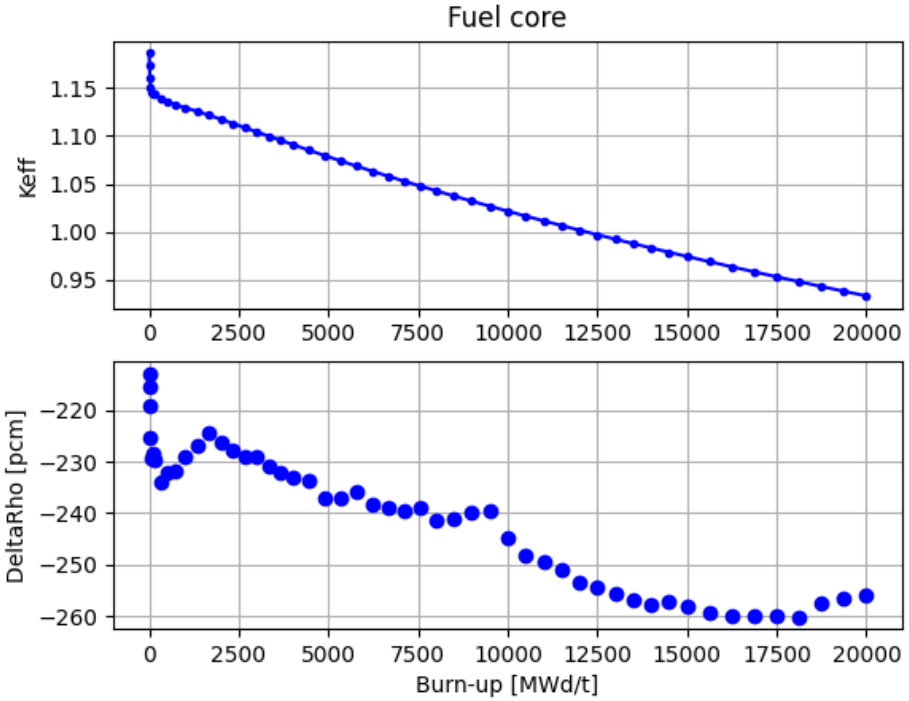

Figure 6.6: k_{eff} changes (top) and reactivity discrepancies (bottom) in the course of depletion for the FG case without the refinement of flux calculation mesh.

Summary and perspective

The internship "Implementation of a reference neutronics calculation scheme with depletion for PWR cores" carried out at CEA Saclay centered on the implementation of a complete and generic scheme using the computational methodology MOC SHEM 281 and testing different method for the self-shielding evaluation with the APOLLO3® deterministic code. This involved a comprehensive comparison with analogous outcomes generated by APOLLO2 for verification and validation.
The scheme is tested on simpler preliminary cases before being developed for the core, thus having a first feedback of the results and first test of the calculation of self-shielding in series on subdomains.
For these cases the FULL EXACT (FE) method is examined, in which the self-shielding is evaluated on the whole geometry using the less approximated TDT-Pij approach, and for this it is the reference case. Among the various methods performing serial and independent self-shielding calculations on subdomains, significant emphasis is placed on the FLUXGROUPEMENT (FG) method.
This method involves computing self-shielding on subdomains with Multicell Pij technique, grouping similar cells based on their configurations and therefore their behaviour. Some important aspects have come out of these studies.
With regard to the first preliminary case, cluster 9x9, it is verified that, using the FG method having more overlapping geometries (cells, sub-clusters and final clusters), the link between the media of the self-shielding and those of the neutron flux is lost and, during the various steps of depletion, the concentration of isotopes is not automatically and correctly updated for each zone.
As a result, a set of functions had to be implemented directly in the data-set to create the match between the flux and the self-shielding calculations. Without the use of these functions, the discrepancy of the k_{eff} values between the two implemented methods exceeds 50 pcm; on the contrary, using this update scheme, the results of FE and FG are not so divergent, less than 10 pcm of difference.
About the second preliminary case of the assembly 17x17, was useful to test the scheme and correct some errors; as a core component, it was important to verify the performance of both methods (FE and FG) for this geometry in steady-state (burn-up = 0) and also in depletion.
Comparing the results with those of APOLLO2, it is clear that the implementation of the calculation scheme is correct and in particular it can be found that using the FG method the computational time is much lower.
Given the good results, the main case of the core is studied. As for the calculation in steady state, methods FE, SM, and FG are tested and verified that compared

to the calculation with the code of the previous generation have little discrepancy, below 20 pcm. For the calculation in depletion instead, remembering that the computation time for self-shielding increases with each step, the only possible method is that of FLUXGROUPEMENT which highlights a good performance in terms of results and calculation time.
Therefore, calculating the self-shielding in series on subdomains, it is clear that, although the greater approximation, the discrepancy of the results compared to the reference case is not so high, but at the same moment the computational cost is significantly reduced.
The forthcoming steps in this study are geared towards the evaluation of the updated version of APOLLO3® and the incorporation of the innovative Isotalo function [20]. This function holds the potential to significantly streamline the depletion analysis process by minimizing the number of required depletion steps for core investigations. By harnessing Isotalo's capabilities, the research aims to enhance the computational efficiency of core analysis, paving the way for more intricate and insightful investigations into reactor behavior and performance. This forward-looking approach underscores the continuous pursuit of advanced techniques to streamline and optimize the analysis of complex nuclear systems.

Bibliography

[1] *CEA. The CEA: a key player in technological research.* 2023.

[2] *Service d'etude des reacteurs et de mathematiques appliquees (SERMA).* 2023.

[3] Milan Hanuš. "Mathematical modeling of neutron transport". PhD thesis. PhD thesis, University of West Bohemia, 2014.

[4] George I Bell and Samuel Glasstone. *Nuclear reactor theory.* Tech. rep. US Atomic Energy Commission, Washington, DC (United States), 1970.

[5] Anil K Prinja and Edward W Larsen. *General Principles of Neutron Transport.* Springer Nature, 2010.

[6] James J Duderstadt and Louis J Hamilton. *Nuclear reactor analysis.* Wiley, 1976.

[7] Elmer E Lewis. *Fundamentals of nuclear reactor physics.* Elsevier, 2008.

[8] B Garland. *Reactor Physics: Multigroup Diffusion.* 2005.

[9] Jerzy Cetnar. "General solution of Bateman equations for nuclear transmutations". In: *Annals of Nuclear Energy* 33.7 (2006), pp. 640–645.

[10] Jean-François Parisot and France, eds. *Neutronics.* DEN monograph. Paris: Editions Le Moniteur, 2015. 273 pp.

[11] Igor Zmijarevic. *Note générale des solveurs de transport du code APOLLO3®.* Tech. rep. CEA, Commissariat à l'énergie atomique et aux énergies alternatives, Paris-Saclay (France).

[12] John R. Lamarsh and Anthony John Baratta. *Introduction to nuclear engineering.* 3rd ed. Addison-Wesley series in nuclear science and engineering. Upper Saddle River, N.J: Prentice Hall, 2001. 783 pp.

[13] Alain Hébert. *Applied Reactor Physics.* 3rd ed. Presses internationales Polytechnique, 2020.

[14] TRIPOLI4® project team. *TRIPOLI4® version 10 user guide.* Tech. rep. CEA, Commissariat à l'énergie atomique et aux énergies alternatives, Paris-Saclay (France).

[15] Didier Schneider et al. "APOLLO3® CEA/DEN deterministic multi-purpose code for reactor physics analysis". In: *PHYSOR 2016–Unifying Theory and Experiments in the 21st Century.* 2016.

[16] V Jouault, J-M Palau, and G Rimpault. "New calculation method for PWR control rod assemblies with APOLLO3®". In: *Annals of Nuclear Energy* 110 (2017), pp. 282–289.

[17] Jean-François Vidal et al. "New Reference APOLLO3® Calculation Scheme for Light Water Reactors–Analysis of the BEAVRS Benchmark". In: *EPJ Web of Conferences*. Vol. 247. EDP Sciences. 2021, p. 06031.

[18] A Santamarina et al. "The JEFF-3.1. 1 nuclear data library". In: *JEFF report* 22.10.2 (2009), p. 2.

[19] Daniele Tomatis et al. "Overview of SERMA's Graphical User Interfaces for Lattice Transport Calculations". In: *Energies* 15 (2022).

[20] A E Isotalo et al. *Flux Renormalization in Constant Power Burnup Calculations*. Elsevier, 2016.